2-16-2018

# Nanoparticle Chemical Sensors: A Study on Optical Humidity Sensor Design

Ross Bradely Chongson
*Rose-Hulman Institute of Technology*

# Nanoparticle Chemical Sensors:

# A Study on Optical Humidity Sensor Design

A Thesis

Submitted to the Faculty

of

Rose-Hulman Institute of Technology

by

Ross Bradley Chongson

In Partial Fulfillment of the Requirements for the Degree

of

Master of Science in Chemical Engineering

March 2018

**ROSE-HULMAN INSTITUTE OF TECHNOLOGY**

**Final Examination Report**

**Ross Chongson** — Name

**Chemical Engineering** — Graduate Major

Thesis Title **Nanoparticle Chemical Sensors: A Study on Optical Humidity Sensor Design**

**DATE OF EXAM:** **February 16, 2018**

**EXAMINATION COMMITTEE:**

| | Thesis Advisory Committee | Department |
|---|---|---|
| Thesis Advisor: | **Adam Nolte** | **CHE** |
| | **Atanas Serbezov** | **CHE** |
| | **Maarij Syed** | **PHOE** |
| | | |
| | | |

**PASSED** X **FAILED** _____

# ABSTRACT

Chongson, Ross Bradley

M.S.Ch.E

Rose-Hulman Institute of Technology

March 2018

Nanoparticle Chemical Sensors: A Study on Optical Humidity Sensor Design

Thesis Advisor: Adam J. Nolte

The need for sensors capable of operating in harsh environments such as those containing flammable, corrosive or reactive vapors is a niche which thin-film optical devices, with their robustness and ease of maintenance may effectively fill. Two such systems were developed using spin-coating techniques and evaluated for applicability as humidity sensors. The first is based on aggregated silica nanoparticles. The second is a polyelectrolyte multilayer film impregnated with silver nanoparticles which exhibited strong surface plasmon response. Ellipsometric experiments performed using a sealed test cell with constant humidity maintained using saturated salt solutions showed that the former responded strongly to changing humidity. The latter possessed interesting hysteresis behavior as analyzed in a climate-controlled glovebox via reflectometry, but proved insufficiently responsive to changing humidity. The silica nanoparticle substrate was found to be a simple, tunable sensor platform which may be viable for the detection of a wide variety of vapor-phase chemical species.

Keywords: Humidity Sensors, Thin Films, Optics, Smart Materials, Spin Coating

## ACKNOWLEDGEMENTS

I would like to acknowledge the support of my family, who gave me the strength and fortitude to see this project through to the very end. I would especially like to acknowledge my mother, whose infinite patience is the stuff saints are made of and my father, whose achievements inspire me to strive more each and every day. I would also like to express my sincerest appreciation to my advisory committee, Doctors Adam Nolte, Maarij Syed and Atanas Serbezov who were always available to lend an ear and some advice when the path forward seemed uncertain. My thanks also goes out to the whole Rose-Hulman Community; I could not ask for a better Alma Mater.

This thesis is also dedicated to two very special people. The first is my late grandmother, Ruth McCarthy, who passed away in the Winter of 2016. She never missed a Sunday lunch to tell us all how proud she was of all we had done, and of all the ways we could still do better. The second is Professor Jacques Zakin, whose guidance and mentorship will always be missed. I regret that I did not finish in time to tell you the good news.

# TABLE OF CONTENTS

# LIST OF FIGURES

# LIST OF TABLES

## LIST OF ABBREVIATIONS

| | |
|---|---|
| AFM | Atomic Force Microscopy |
| NP | Nanoparticle |
| PAA | Polyacrylic Acid |
| PAH | Poly(allylamine hydrochloride) |
| PEM | Polyelectrolyte Multilayer |
| QCM | Quartz Crystal Microbalance |
| RH | Relative Humidity |
| RPM | Rotations Per Minute |
| SEM | Scanning Electron Microscopy |
| TEM | Transmission Electron Microscopy |
| SPR | Surface Plasmon Resonance |
| LSPR | Localized Surface Plasmon Resonance |
| UV | Ultraviolet |

## LIST OF SYMBOLS

| | |
|---|---|
| $h_v^{in}$ | Vector of light incident upon the surface of the film |
| $h_v^{ref}$ | Vector of light reflected from the surface of the film |
| $AB$ | Absolute Humidity |
| $RH$ | Relative Humidity |
| V | Volume |
| $P_w$ | Partial pressure of water in the ambient environment |
| $P_s$ | Partial pressure of water at saturation |
| $n_w$ | Moles of water in the ambient environment |
| $n_s$ | Moles of water at saturation |
| $m_w$ | Mass of water in the ambient environment |
| $m_s$ | Mass of water at saturation |
| $n$ | Refractive index |
| $d$ | Film thickness |
| $k$ | Extinction coefficient |
| $\phi$ | Angle of incidence or refraction |
| $r_{mp}$ | Amplitude of reflected p-polarized light |
| $r_{ms}$ | Amplitude of reflected s-polarized light |
| $t_{mp}$ | Amplitude of transmitted p-polarized light |
| $t_{ms}$ | Amplitude of transmitted s-polarized light |

| | |
|---|---|
| $\mathbf{R}$ | Reflectance of a film |
| $\mathbf{T}$ | Transmittance of a film |
| $\lambda$ | Wavelength of light |
| $\delta_m$ | $\frac{2\pi n_m d_m cos(\phi_m)}{\lambda}$ |
| $n_{eff}$ | Effective refractive index |
| $n_c$ | Refractive index of material 'c' |
| $n_d$ | Refractive index of material 'd' |
| $f_v$ | Volume fraction of material 'd' |
| $\Delta_f$ | Change in the frequency of the QCM crystal in Hz |
| $\Delta_m$ | Elastic mass change in grams |
| $f_0$ | Intrinsic crystal frequency in Hz |
| $A_e$ | Electrode area in $cm^2$ |
| $\mu$ | Shear modulus |
| $\rho_q$ | Density of quartz |
| $\lambda_s$ | Shear wavelength of a particular medium |
| $\beta_1$ | Limit of Sauerbrey Function for viscous materials |
| $\omega_c$ | Radian frequency of the vibrating crystal |
| $\rho$ | Material density |
| $\eta_M$ | Magnitude of the complex viscosity of the material |
| $\phi_L$ | Relative phase angle of the liquid medium |

| | |
|---|---|
| $\sigma$ | Dielectric function |
| $\sigma_r$ | Real component of the dielectric function |
| $\sigma_s$ | Imaginary component of the dielectric function |
| $\lambda_{exc}$ | Excitation wavelength of a given material |
| $C_{ext}$ | Extinction cross-section of a given material |
| $R_p$ | Particle diameter |
| $\sigma_m$ | Dielectric constant of surrounding medium |
| $A$ | Absorbance in absorption units (a.u.) |
| $T$ | Percent of light transmitted through a medium |

# 1 INTRODUCTION

Sensors play a vital role in all areas of science and industry, and their design is continuously evolving. Since the development of the first commercial thermostat by Warren S. Johnson in 1883, the field has advanced from the use of precision mechanical or thermochemical devices towards the use of electronics.[1] Sensing devices can, today, be found serving applications from the mundane to the extraordinary, from thermal imaging devices in airports to neutrino detectors constructed deep underground.

One particularly useful subset of sensors for a wide range of industries are those developed to measure humidity. Water vapor is ubiquitous. Its concentration in the local environment has a significant effect on everything from the decomposition of organic matter in forests to the heat transfer coefficients in large-scale industrial facilities, to simply gauging how uncomfortable it might be to go outside on a hot summer afternoon. It goes without saying that, alongside the thermostat and its ilk, humidity sensors are among the most relevant to day-to-day life.

A particularly vital application of humidity sensing devices is in monitoring and controlling the environmental conditions in laboratory settings. Many reactions are highly sensitive to the amount of moisture in the local environment, and a wide assortment of sensitive instruments are susceptible to damage or malfunction under sufficiently humid conditions. In such scenarios, it is highly desirable to be able to continuously monitor and control the levels of ambient humidity, making sensors capable of doing so with minimal hysteretic effects and high response time invaluable.[2, 3, 4, 5]

Of the sensors presently on the market, most operate via some measurement of electronic behavior, often either capacitance or impedance. However, there exists an interesting possibility for the development of optical humidity sensors, many of which are conceptually robust enough to be extended- with some modification- into detecting the presence of specific chemicals within the local environment. The use of optics as a vector for humidity sensing is not entirely novel- absolute humidity sensors based on water condensation on a mirror were developed as early as 1948.[6] The design was further improved in 1967 by Jury et al.[7] As their name suggests, these devices measure some change in the optical properties of some subject system and thus correlate that data to a change in local humidity. For instance, one might be able to detect the influence of humidity on the refractive index or maximum absorption wavelength of a thin film, and by this correlation, determine the relative humidity in the ambient environment. Either of these systems are easily monitored through standard reflectometric or ellipsometric methods. Provided the proper models are in place to correlate these changes to shifts in environmental conditions, these devices could prove to be a useful resource, especially when the use of electronic circuits is not necessarily ideal.

Some of the most appealing materials for the development of such devices are, indeed, thin-films. These have been the focus of some of the most important research in materials science within the past several decades, serving to advance our knowledge and design of a whole host of useful technologies. Furthermore, thin films possess an array of qualities that make them ideal for the sensing of changes in environmental conditions, such as:

1: Rapid response times: Thin films possess a very high surface to volume ratio. Thus any change to ambient conditions propagates rapidly through the bulk of the film, barring the integration of some inhibitory measure.

2: Tunable Optical Properties: By adjusting the variables involved in the fabrication process, we

are capable of producing thin films with properties that best suit the designated task.

3: Robustness: Depending on the design, films can often be made quite durable and robust. We can also achieve impressive chemical robustness so long as we choose appropriate materials, allowing the use of these devices in a wide range of environments.

4: Simplicity of Manufacture: While the development of highly complex, multi-component multilayer films is a subject of much study, many thin films are remarkably simple. Single-layer and simple multilayer films can easily be produced by spin-coating or dip-coating methods. The former is particularly effective at rapidly producing highly uniform films, making it ideal for high-throughput production schema.

These advantages are not restricted to the application of thin film regimes to optical systems. That is, thin films and especially sensor-on-a-chip apparatuses are equally advantageous for both the conventional electronic humidity sensors as well as the hypothetical optical humidity sensors presented herein. The motivation for investigating the latter has emerged as a result of an interest in distributed sensor arrays and the cost-saving measures that photonic systems might provide to such networks.

Take, for instance, a situation where we might want to monitor the humidity or chemical vapor concentrations at multiple different locations within a single process flow. While such a system could be achieved by using multiple electronic sensors distributed at each of the target sites, doing so would necessitate the purchase, installation and maintenance of however many electronic sensors that the process would call for. By comparison, we could instead install multiple optical sensors based on robust glass slides or other chip-based setups at each of the target locations. Each of these chips could be monitored by one (in the case of reflective sensing) or two (in the case of ellipsometric or transmission-based sensing) optical fibers that would feed from a single light source to a single sensor,

both of which could be located as near or as far from the site of detection as desired.

Optical fiber cables provide impressive durability and significant resistance to a wide variety of chemical environments. They are further capable of operating at significantly higher temperatures than electronic systems; commercially available borosilicate glass fibers (from fiberopticstech) can continue to function up to 482°C, and one sapphire-ruby fiber developed in 2001 can function up to 1500°C.[8] Comparatively, many electronic systems tend to have an upper limit of approximately 180-200°C.[9] If combined with a similarly robust sensor chip, we would be capable not only of monitoring multiple locations with a single sensor, but those locations could also be exposed to significantly more extreme environments than traditional electronic systems while simultaneously isolating the relatively more delicate electronics in a location that is both easily accessed and isolated from factors which may inhibit or damage their function. This is particularly useful when flammable or corrosive vapors are a possible liability, not only improving safety but also reducing the frequency of maintenance and repair.

Compared to their electronic cousins, optical humidity sensors have the potential to be significantly more durable and resilient. Silica systems, for instance, are incredibly chemically robust. Utilizing a silica-based schema to develop a humidity sensor- and indeed, chemical sensors in general- allows us to take advantage of this property, while still also making use of silica's highly tunable surface chemistry. While historically considered to be less than ideal in their unmodified state for electronic humidity sensing due to their high intrinsic electrical resistance, silica nanoparticle films can be highly hydrophilic. This provides a promising basis for the development of an optical humidity sensor.[10, 11, 12, 13] Moreover, the wide range of surface modifications being studied or applied in literature suggests the possibility of utilizing silica as a launch-pad for the development of an assortment of chemical sensors in general.[14, 15, 16] The use of an optical, thin-film device can

also serve as a cost-saving measure. Compared to conventional, electronic humidity sensors, the components of an optical sensor most frequently exposed to the local environment can be cheap and simple to manufacture. Single-layer silica films can be produced en masse at a relatively low cost, for example. While the electronics and optical equipment required to operate these sensors may pose a higher up-front cost, loss may be recuperated in a reduction in maintenance.

Pre- and post-processing techniques allow us to modify these films further. This can include controlling critical properties such as thickness, porosity and so on by manipulating the conditions under which the films are prepared. For instance, we might be able to generate a more or less densely packed nanoparticle film based on how long we expose the precursor to elevated temperatures. In another case, we may wish to lower the pH of a polymer precursor to increase the available charged sites within the film. [17, 18, 19, 20]

The surfaces of the prepared film might also be patterned for more advantageous optical properties. Alternately, we could modify the surface chemistry, changing how they might respond to certain environmental stimuli. It may be possible, using these methods, to modify a basic film structure in such a way that it absorbs only molecules containing a target functional group. The design of such a sensor is beyond the scope of this research, though it presents a compelling path for future investigation.[14, 15, 16]

The goal of this thesis is to present a solution to some of the problems faced by conventional electronic humidity sensors in the form of an optical alternative. In order to do so, we will examine and present two methods by which an optical humidity sensor might be developed focusing specifically on comparing a porous silica monolayer system developed via a single-step spin deposition method to a poly(allylamine hydrochloride)/polyacrylic acid (PAH/PAA) polyelectrolyte multilayer film prepared by a layer-by-layer deposition method and infused with silver nanoparticles.

These systems serve as useful case-studies for two different mechanisms of optical humidity sensing. In the case of the silica, we will be exploring how changes in ambient humidity can be correlated to shifts in the refractive index of a film that results from the infiltration of water into the films interparticle voids. The polyelectrolyte multilayer, with its unique absorption-desorption and swelling behavior is an interesting environment for investigating the way in which humidity can affect the surface plasmon resonance (SPR) frequency of the silver nanoparticles suspended within. A simplified diagram of the two schemes can be seen below in Figures 1.1 and 1.2.

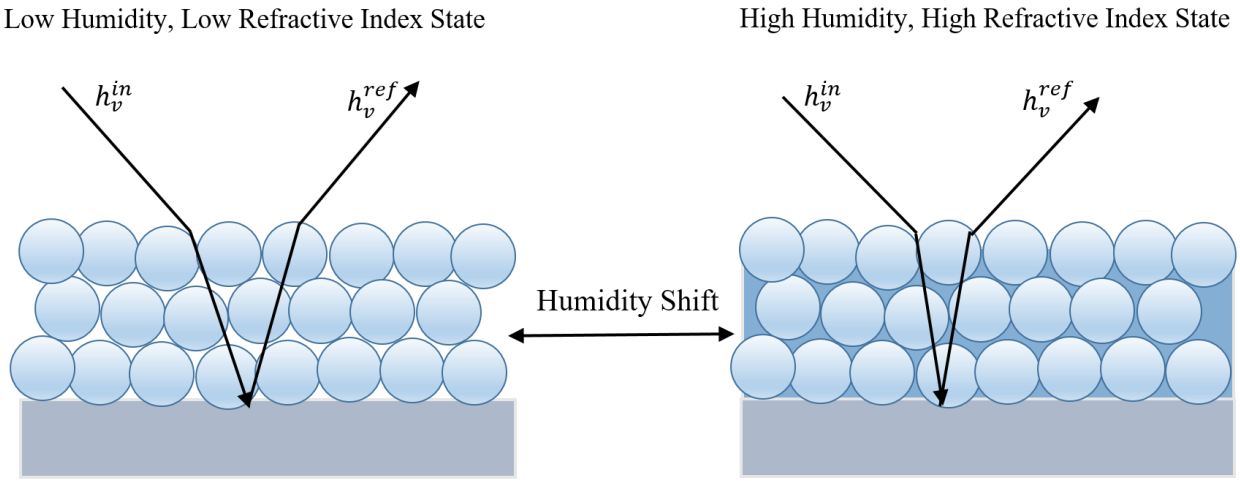


Figure 1.1: Simplified diagram of silica nanoparticle (blue-grey) based optical humidity sensor on silicon (grey) substrate. Note change in angle of refraction between upon hydration, typically detectable only with a non-zero angle of incidence. However, the addition of water into the interparticle voids affects the refractive index, which in turn affects the optical path length which can be captured via reflectometry.

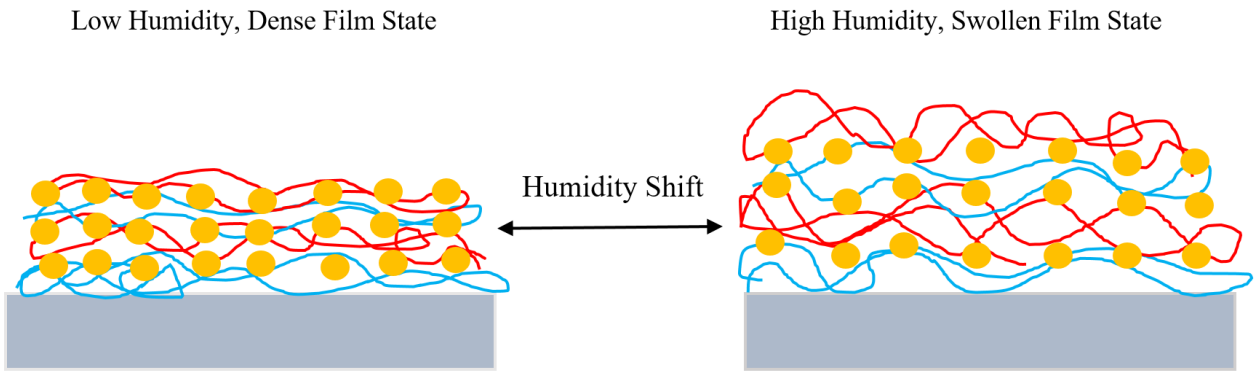


Figure 1.2: Simplified diagram of humidity sensor based on a PAH (blue)/PAA (red) polyelectrolyte multilayer film infused with silver nanoparticles (orange) on silicon (grey) substrate.

These two devices will be explored throughout four chapters of this thesis. Chapter 2 will outline the background of conventional electronic sensors in more detail, and will further elaborate on the potential use of an optics-based sensor as an alternative. This segues into a literature review on the present state of humidity sensing devices.

With the general overview complete, Chapter 3 and 4 will then delve into background information specifically pertaining to silica nanoparticle and polyelectrolyte multilayer films respectively. They will also explore some of the specific optical and physical properties being examined as humidity changes. These chapters will also provide a description of the methodologies used to investigate both film stacks. Lastly, these chapters will contain an analysis of the experimental results gleaned from study into the two devices.

Finally, Chapter 5 will end the thesis with a summary of the experimental results. It will also present a look into what future research might be done to extend the work presented here further.

# 2 HUMIDITY SENSORS

## 2.1 A Primer on Humidity

In simplest terms, humidity is a measurement of the concentration of water vapor in the local atmosphere. There are a number of different ways to quantify humidity, which Farahani et al. cover effectively in their review of the topic, but which will be paraphrased here for future reference.[13] The first of these is the direct measurement of the mass of water per volume, which is one of the representations of absolute humidity (AB). Absolute humidity is typically presented in units that immediately evolve from primary measurement, such as grams or parts-per-million. Thus, AB can be represented as:

$$AB = \frac{m_w}{V} \tag{2.1}$$

Where $m_w$ is the mass of water in the designated volume, V.

Another method is by use of relative humidity (RH), which is defined by a ratio of measured moisture content relative to the maximum concentration of water vapor at saturation for a given temperature and pressure. Relative humidity is dimensionless, and is frequently represented as a percentage based on partial pressures, such that:

$$\frac{RH}{100\%} = \frac{P_w}{P_s} = \frac{n_w}{n_s} = \frac{m_w}{m_s} \tag{2.2}$$

Where P denotes a partial pressure, n denotes moles and m mass. Subscript w denotes measured values in the ambient environment and subscript s denotes a value at saturation at a given temperature and pressure.

The last conventional measurement of humidity are the dew and frost points. Dew point is defined as the temperature that suspended water vapor will begin to condense into liquid form. Frost point is similar- a temperature at which water vapor condenses into ice. These are typically used for absolute humidity measurements because they are dependent solely on the pressure of the gas in question. Other measurements of absolute humidity are typically performed by mass measurement or by directly sampling the volume fraction of water in a sample of gas.

All humidity sensors will measure ambient humidity based on one of these definitions. In most cases, however, relative humidity sensors are often simpler and cheaper to design.[21, 22, 23] Indeed, this is reflected in industry- a vast majority of humidity sensors in use today are based on relative humidity, even those used in laboratories. It is of course preferable to acquire absolute humidity data when, for instance, an experiment calls directly for the mass of water vapor in a certain volume of gas. Thus, absolute humidity devices still have a number of applications for specialized experimentation.

## 2.2 Current Relative Humidity Sensors

While there are a number of different humidity sensors on the market, each device falls into certain categories based either on the type of humidity being measured (relative or absolute), the type of material used or the electrical property being probed to measure changes in humidity. As categorized

in 2005 by Chen and Lu, most relative humidity sensors can be classified as one of three different classes, based on the types of materials from which they are constructed.[15] These material classes include ceramics, semiconductors and polymers. Beginning then with the first of the three primarily used in the industry:

### 2.2.1 Ceramics

This category is comprised of all manner of inorganic, non-semiconductive compounds which operate by means of adsorbing water vapor from the local environment onto their surfaces, whether by physisorption, chemisorption or capillary condensation.[15, 16] In addition to the standard mode of electrical conductivity which needs little elaboration, these materials also function via ionic conduction of hydrogen and hydroxide ions. This by taking advantage of the Grotthuss mechanism and Grotthuss hydroxide transfer respectively.[24, 15]

The mechanism for hydrogen ion conduction in liquid water was first introduced over 200 years ago in 1806 by Theodor von Grotthuss, who described what would later be named the Grotthuss Mechanism.[24] In this mechanism, hydrogen ions essentially jump from one water molecule to the next as shown in Figure 2.1.[24] The basic mechanism can be summarized as a sort of 'bucket line.' Hydrogen ions hop from one water molecule to another, temporarily forming an unstable hydronium ion. One of this ion's surplus hydrogens then jumps to another neighboring water molecule, causing a propagating 'wave' or 'current' of hydronium ions through a body of water. Hydroxide ions can also migrate through the film through a comparable mechanism. Hydroxide ions may migrate by colliding with adjacent water molecules and taking up one of its hydrogens. This produces a new hydroxide ion that may then go on to react with another adjacent water molecule, and so on. Thus a hydroxide ion 'travels' through water in much the same way as the hydrogen ion described above.

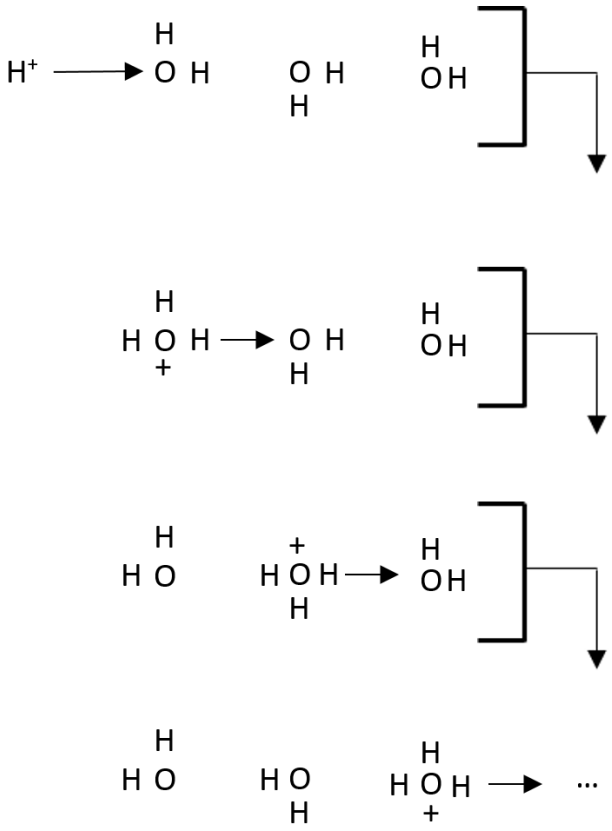

Figure 2.1: Basic Outline of Grothuss Mechanism.

In essence, ceramic materials act as a hydrophilic surface upon which layers of water may form; as these layers accumulate, conductivity tends to increase. When first exposed to a humid environment, water molecules come into contact with the ceramic surface, and complex with the metal-oxide network at its surface. Soon afterwards, this complex breaks down, covering the surface of the substrate with surface hydroxyl groups. Following this, another layer of water forms; this second layer is effectively immobilized by the hydrogen-oxygen attraction between the hydroxyl end groups and the oxygen within the water molecules. At this point, the system is unable to allow the transport of hydrogen ions as none have yet been produced by water-water interactions. However, any additional layers of water adsorbed onto the substrate surface contain water molecules that are significantly more mobile. These additional layers become capable of releasing protons or hydroxide ions, which both act as charge carriers that cause the system to become more conductive as their concentration increases. This change in conductivity can be measured relatively easily, allowing for the detection of changes in humidity. Ceramic sensors that utilize this mechanism do not operate well under less humid conditions. The lack of water molecules in such environments prevents the formation of additional layers upon the substrate. This in turn prevents the formation of hydrogen ions and prevents us from using this method to accurately probe such low levels of humidity.[21, 23, 25, 26]

### 2.2.2 Semiconductors

Many semiconductor-based sensors in fact utilize ceramic oxides such as those outlined previously. $SnO_2$, $In_2O_3$ and $ZnO$ are all commonly used ceramic oxides that exhibit wide-bandgap semiconductivity. Semiconductor-based sensors are theorized to operate based on principles not too dissimilar to that of the ceramics. When water is adsorbed onto the surface of a semiconductive substrate, we observe an increase in the conductivity of n-type substrates while decreasing the conductivity of p-types.

This is thought to be due to one of several mechanisms: the first suggests that electrons are being donated by chemically absorbed water into the semiconductor, the second suggests that water molecules displace oxygen ions from the surface upon adsorption. When these ions react to form oxygen gas, they release their electrons into the semiconductor. These two factors involve electron donation, and account for the different response of n- and p-type semiconductors to water adsorption.[14, 16]

Semiconductor sensors are also capable of operating at significantly higher temperatures than other devices. Many of the studies associated with them have focused on temperature ranges well above 100C. This is due to the fact that the sensors operate primarily via chemisorption rather than physisorption mechanisms. That is, its only needed for water molecules to interact with the sensors surface; further layers are unneeded. Thus, even at elevated temperatures that would make the accumulation of additional water layers impossible, the semiconductor humidity sensors would still be able to produce useful data.[15]

### 2.2.3 Polymers

Polymer sensors are typically deposited as thin films as well. These electronic sensors operate either by observing a change in the electrical conductivity as a response to changes in humidity, or by observing changes in capacitance. Due to the relatively low melting point of most polymers, these systems typically operate near room temperature. This also limits their operating ranges; unlike ceramic or nanoparticle sensors, polymer sensors are highly susceptible to damage due to heat.[14, 15, 16] Most of the resistive sensors are based on hydrophilic polyelectrolytes which were organized by Chen and Liu into three primary classifications based on their functional electrolytic groups. These categories are quaternary ammonium salts, sulfonate salts and phosphonium salts.[15]

When water enters these films, it raises the mobility of the aforementioned charge carriers, while

also possibly dissociating- as in the ceramic sensors- into hydrogen and hydroxide ions. This latter behavior increases the total concentration of charge carriers in the film. These two effects contribute to an increase in conductivity.[22, 23]

That said, these films are quite susceptible to damage due to their high water solubility; with regular exposure to high levels of humidity, research has shown a degradation in the sensitivity and efficacy of polyelectrolyte sensors.[27, 21] Furthermore, they also have a tendency to be insensitive to changes at high relative humidity (above 50% RH) and exhibit strong hysteresis, the latter which may be due to the accumulation of water in interstitial pockets within the films; as humidity decreases, the mechanism for the evaporation of this water may be substantially different from that of its deposition.[14, 15, 27] We can, however, reduce hysteresis by crosslinking the polymer network, resulting in stiffer and more chemically robust films, though this does little to improve responsiveness at high RH. [27, 28]

Research has suggested that conjugated, conductive polymers such as poly(3,4-ethylene-dioxythiophene) (PEDOT) or poly(3,4-ethylenedioxythio phene)-poly(styrene-sulfonate) (PEDOT-PSS) can exhibit higher durability, lower hysteresis and higher sensitivity as well.[29, 30] Depending on how they're tuned, these sensors can exhibit effective linear response between 10% to 90% RH, though they are still somewhat limited by their allowable operating temperature.

The other category of polymer sensors rely on capacitance. For these systems, its ideal to use more hydrophogic polymers that are still capable of absorbing water such as polyimides, poly(methylmethacrylate) (PMMA) and poly(ethyleneterephthalate) (PET).[27, 21, 26, 31, 32] These sensors see wide applicability in industry due to their relative ease of production, highly linear response, high stability and other useful properties.[13, 15] This is due to the mechanism by which the capacitance of the system is thought to change. These materials tend to have physical properties, such as dielectric constant,

permittivity, etc, which change proportionally to the amount of water absorbed into the system. The changes in these physical properties can be directly measured via capacitance.[33] In general, the sensitivity and the response time of these capacitive sensors can be improved significantly by increasing the porosity of the films due to increasing the permeability to water vapor.[34]

Though their structural properties and relatively low cost make these sensors attractive alternatives, hysteresis is a significant issue associated with their use.[35] Its thought that this may be due to deformations in the polymer by the accumulation of clusters of water within the network. This deformation may detrimentally affect the performance of the transducer, and depending on the flexibility of the polymer, can vary substantially between humidity states.

Another class, the organic/inorganic composite material sensors has been described by Parvatikar, as well as Tandon and several other researchers.[36, 37, 38, 39] As the name implies, these devices utilize a combination of organic and inorganic materials to produce a single system with more attractive material properties. Some of the most interesting work in this field has been in the development of polymer-nanoparticle film systems.[40, 41]

These devices have been reported to possess nearly linear response between 11-95% relative humidity, minimal hysteresis and faster response times than equivalent devices developed solely from either polymer or ceramic systems. It is believed that this is due to a two-fold humidity response mechanism. When operating under low humidity, the devices primarily rely on the electron exchange from absorbed water molecules. At higher humidity, a mechanism similar to the Grotthuss mechanism dominates, and the primary charge carriers become hydrogen ions being exchanged between water molecules. In essence, combining polymers and ceramics have produced devices with greater sensing capabilities than either material could achieve alone.

### 2.2.4 Temperature Limitations

As long as the temperature exceeds the boiling point, it is nearly impossible to acquire reasonable data on the amount of water vapor present in an environment, as very little of it will be remain adsorbed onto the surface of the sensor. However, this does not mean that water is not still found within the sensor itself; while water cannot physisorb onto sensors above the boiling point, we can still observe chemisorption of water. That is, despite elevated temperatures, sensors can still detect the presence of water via the concentration of hydroxyl groups into an extremely small ($< 1$ nm) region on their surface, as described by Morimoto et al.[42]

Due to the small size of these chemisorbed regions, its unlikely that an optical method would be able to detect their presence. However, this does not discount an optical mode of measurement as a useful tool; indeed, this limitation is quite notably dependent not only on temperature, but on pressure as well. Depending on the situation, it may be that a high pressure/high temperature environment might still allow for an optical sensor to function more effectively than an electronic counterpart. Furthermore, for most applications where distributed humidity sensing would be desirable, operation at extremely high temperatures is unnecessary.

## 2.3 Optical Humidity Sensors

As previously mentioned, the sensors that are the subject of this thesis are hardly the first optical humidity sensors to be developed. The first such devices were developed in order to monitor the absolute humidity at extremely dry conditions. A device known as a chilled mirror hygrometer was developed by Brewer et al. in 1948 and was specifically designed to sense the humidity of air located in the stratosphere.[6] In essence, the mechanism operates as follows:

A light source is projected onto the sensing element, which in this case is some kind of mirror (gold is particularly common due to its well-studied optical properties) and is subsequently received by the photoresistor. Should any water condense or freeze across the surface of the mirror, the signal detected by the photoresistor will decrease in intensity as the amount of light reflected from the surface drops. Comparing the change in signal to the temperature of the mirror, we can establish the dew point- and thus, we can evaluate how much moisture exists in the target environment.

While the earliest such designs relied largely on ambient temperature, evolutions in the technology produced devices that could regulate and stabilize the temperature of the sensing element, thus allowing for greater control.[7] Later designs also separated the light source from the sensing element by use of optical fibers to ensure that the temperature control system did not influence the detector. In all, these devices were found to be capable of isolating the dew point to within around 0.10°C, though they also had rather slow response times compared to their electronic cousins. Furthermore, the devices suffered from their high cost, instability over long periods of time and a tendency for the sensing element to be contaminated by compounds within the local environment. They were, however, also among the few devices capable of measuring absolute humidity rather than simply monitoring relative humidity.

The sensors studied in this thesis will be taking advantage of similar principles to these devices. However, rather than using a simple mirror, the sensing element in these devices will exploit a variety of advantages afforded by their unique physical and material properties in order to improve both the effectiveness and economics of the optical method. As previously mentioned, the two properties we will be investigating are the refractive index of a silica nanoparticle film and the SPR frequency of silver nanoparticles grown within a polyelectrolyte film.

As an important note, however, the sensors that this thesis will investigate were evaluated solely

based on their ability to detect changes in relative humidity. While it may be possible to detect changes in absolute humidity using these devices- and indeed, that is a possible avenue for further study- relative humidity is both easier to gauge and more practical to use for most situations.

### 2.3.1 Optical Properties of Thin Films

O. S. Heavens' comprehensive article on the optical properties of thin films was published in 1960 and has largely informed my understanding of the subject.[43] Speaking in generalities, the optical properties of thin films are dominated by three major variables: the refractive index (n), the thickness of the film (d) and the extinction coefficient (k). This latter variable is only useful when considering a film which tends to absorb light, however. As both the silica film and the polyelectrolyte multilayer (prior to introduction of silver NPs) should not absorb a great deal of light, we can assume that k is close enough to zero that it can be ignored. However, if it were not, then we would need to use a complex n defined as:

$$\mathbf{n} = n - ik$$

We must analyze either the reflectivity or the transmittivity of the material in order to piece out these variables. When performing such analyses, we must take into account that light which is incident to a surface at any angle but perpendicular to that surface must be broken down into parallel (p) or senkrecht (s, perpendicular) polarizations. It is thus important to account for the angles ($\phi$) of incidence and refraction as well. For brevity's sake, the angle of incidence will be denoted by a phi with the subscript 'm', and the angle of refraction by a phi with the subscript 'm-1'. In essence, these are the angles at which light approaches and emerges from an interface respectively, and are related by Snell's law:

$$n_m sin(\phi_m) = n_{m-1} sin(\phi_{m-1}) \tag{2.3}$$

The Fresnel coefficients are defined as the ratio of reflected ($r_m$) or transmitted ($t_m$) amplitude to incident amplitude and are key in calculating reflectance and transmittance. For a single-layered film exposed to a surrounding medium, we define the Fresnel coefficients as the following. For the p-component:

$$r_{mp} = \frac{n_m cos(\phi_{m-1}) - n_{m-1} cos(\phi_m)}{n_m cos(\phi_{m-1}) + n_{m-1} cos(\phi_m)} \tag{2.4}$$

$$t_{mp} = \frac{2n_m cos(\phi_m)}{n_m cos(\phi_{m-1}) + n_{m-1} cos(\phi_m)} \tag{2.5}$$

And for the s-component:

$$r_{ms} = \frac{n_m cos(\phi_m) - n_{m-1} cos(\phi_{m-1})}{n_m cos(\phi_m) + n_{m-1} cos(\phi_{m-1})} \tag{2.6}$$

$$t_{ms} = \frac{2n_m cos(\phi_m)}{n_m cos(\phi_m) + n_{m-1} cos(\phi_{m-1})} \tag{2.7}$$

We can see that in the case where the incoming light is incident at an angle perpendicular to the surface, the results from the s and p polarized formulae are equal and can be simplified as:

$$r_m = \frac{n_m - n_{m-1}}{n_m + n_{m-1}} \tag{2.8}$$

$$t_m = \frac{2n_m}{n_m + n_{m-1}} \tag{2.9}$$

Assuming that we have only a single film in our stack, we can finally define the reflectance and transmittance and incorporate the film's thickness into the calculation.

The reflectance ($\mathbf{R}$) and transmittance ($\mathbf{T}$) of the film can then be defined as:

$$\mathbf{R} = \frac{r_m^2 + 2r_m r_{m+1} cos(2) + r_{m+1}^2}{1 + 2r_m r_{m+1} cos(2\delta_m) + r_m^2 r_{m+1}^2} \tag{2.10}$$

$$\mathbf{T} = \frac{n_{m+1}}{n_{m-1}} \frac{t_m^2 + t_{m+1}^2}{1 + 2r_m r_{m+1} cos(2\delta_m) + r_m^2 r_{m+1}^2} \tag{2.11}$$

Where $\delta_m = \frac{2\pi n_m d_m cos(\phi_m)}{\lambda}$ and $\lambda$ is the wavelength of the incident light.

These are the reflectance and transmission which we measure experimentally. However, it is important to note that we measure both of these as a spectrum. It is more accurate to describe $\mathbf{R}$ and $\mathbf{T}$ as functions of the wavelength, such that: $\mathbf{R} = \mathbf{R}(\lambda)$ and $\mathbf{T} = \mathbf{T}(\lambda)$. This dispersion is a well-known phenomenon, and a number of models exist to describe the relationship between refractive index and wavelength. The most well-known is likely Cauchy's equation, developed nearly two-hundred years ago in 1830 by Augustin-Louis Cauchy. Cauchy's equation is typically represented as:

$$n(\lambda) = A + \frac{B}{\lambda^2} + \frac{C}{\lambda^4} + ... \tag{2.12}$$

Where A, B, C and so on are empirically derived constants specific to particular material.[44]

Cauchy's equation is only accurate for wavelengths in the visible spectrum, specifically between 365.0 and 1013.9 nm.[45] Sellmeier developed another model based on Cauchy's work which is accurate from ultraviolet to infrared and is described as:

$$n(\lambda)^2 = 1 + \frac{B_1\lambda^2}{\lambda^2 - C_1} + \frac{B_2\lambda^2}{\lambda^2 - C_2} + \frac{B_3\lambda^2}{\lambda^2 - C_3} + ... \tag{2.13}$$

Where $B_n$ and $C_n$ are empirically derived, material-specific constants.[46]

Because the measurements of interest taken by our instruments are limited to the visible range, Cauchy's model will suffice for our analysis. The silica nanoparticle film requires an additional model in order to properly analyze the uptake of moisture into the film's pores. To this end, we will need to apply an Effective Medium Approximation (EMA) model.

### 2.3.2 EMA Models

The EMA models are typically used to analyze the optical and dielectric properties of porous or multiphase media. Cook et al. previously analyzed these films using three different EMA models.[18] The first is simple weighted index or Birchak model, which approximates the material's porosity by assuming each material contributes in equal proportions to the combined refractive index.[47]

The second model is the dielectric-weighted or Yoldas (or Silberstein) model.[48, 47] While this model still uses a volumetric ratios of the components in the material to compute the mixed refractive index, it instead applies the aforementioned ratios to the optical dielectric constants of the materials– that is, the square of the refractive index.

The third model, the Symmetric Bruggeman is similar to the first in that it weights both phases

equally. However, it is distinct in that it considers each phase's permittivity relative to that of the whole material.[49] Rather than comparing, say, the silica's refractive index to that of the void, it instead compares them both to that of the material that they are components to. In this way, each phase is treated as part of a whole, with each component contributing to the refractive index based on its volume fraction.

A fourth model, used here to compare against as the gold standard of analyzing the effective refractive index of mesoporous thin films, is the 3D-Maxwell Garnet (MG) model. This model was specifically developed to analyze films with spherical inclusions (in this case, void is the inclusion) and small volume fractions. [47]

The governing equations for each of these models are listed below in order of their introduction.

$$n_{eff} = n_c(1 - f_v) + n_d f_v \tag{2.14}$$

$$n_{eff}^2 = n_c^2(1 - f_v) + n_d^2 f_v \tag{2.15}$$

$$0 = (1 - f_v)\frac{n_c^2 - n_{eff}^2}{n_c^2 + 2n_{eff}^2} + f_v\frac{n_d^2 - n_{eff}^2}{n_d^2 + 2n_{eff}^2} \tag{2.16}$$

$$n_{eff}^2 = n_c^2[1 - \frac{2f_v(n_c^2 - n_d^2)}{n_c^2 + n_d^2 + f_v(n_c^2 - n_d^2)}] \tag{2.17}$$

Where $n_{eff}$ is the effective refractive index of the material as measured, $n_c$ is the refractive index of one material, $n_d$ is the refractive index of the other material and $f_v$ is the volume fraction of the second material, essentially a measure of porosity of the film. In this case, $n_c$ is assumed to be the refractive index of silica at 633 nm, approximately 1.462 as measured by Herzinger et al. This is also used by the CompleteEASE software in the SiO2 JAW model.[50] Here, $n_d$ is assumed to be 1, the

refractive index of air.[18]

In Table 2.1, we compared the refractive indexes as calculated using each of these models of a film spun at 2000 RPM and transferred from room humidity to a humid environment ($\phi_{K_2SO_4} = 98.0\%$) for an hour. This data was found to be consistent even for films spun at speeds other than 2000 RPM.

Table 2.1: Void Fractions of Films Exposed to High Humidity for Certain Lengths of Time as Calculated with (a) The Birchak Model. (b) The Yoldas Model. (c) The Symmetric Bruggeman Model. (d) The 3D Maxwell-Garnet Model.

| Time (mins) | Ref.Index (n) | % Void (a) | % Void (b) | % Void (c) | % Void (d) |
|---|---|---|---|---|---|
| 1 | 1.2895 | 37.34 | 41.73 | 36.19 | 37.07 |
| 2 | 1.2976 | 35.58 | 39.89 | 34.47 | 35.31 |
| 5 | 1.3049 | 34.00 | 38.22 | 32.96 | 33.72 |
| 20 | 1.3192 | 30.91 | 34.92 | 29.97 | 30.62 |
| 60 | 1.3278 | 29.05 | 32.92 | 28.17 | 28.76 |

As seen in Table 2.1, the Birchak, Bruggeman and MG model strongly agree with one another and predict porosities within 0.5% of one another. The Yoldas model predicts consistently higher porosity, but is still within 5% of the other predictions. This is to be somewhat expected, as literature review has shown that the Yoldas model consistently predicts dielectric constants which constitute the upper bound of some data sets owing to its linear behavior.[51] Considering the tight spacing of the other models, it seems reasonable to use only one of those as the basis for our calculations going forward. As such, the Bruggeman model is selected for the silica NP film going forward.

## 2.4 Other Pertinent Backgrounds

### 2.4.1 The QCM

The fundamental principles behind the QCM were first conveyed by the Curie brothers in 1880 when they discovered that quartz crystals held piezoelectric qualities. Lord Rayleigh later showed that a change in a crystals intertia could alter the resonant frequency of its vibrations. These two factors underlie the basic operations of the QCMs critical sensing component: that the crystal oscillates at a certain frequency when exposed to an alternating electric field, and that this characteristic frequency can then be tuned by the addition or removal of mass from the crystal.[52, 53, 54]

It was 1959 when Sauerbrey first reported that the QCM exhibited a linear decline of the frequency, f of an oscillating quartz crystal with the deposition of metal onto the crystal. The relationship he derived, called the Sauerbrey Equation, is still the most commonly used model for the addition of elastic mass to the crystal.[53] The Sauerbrey Equation is as follows:

$$\Delta_f = -\frac{2\Delta_m f_0^2}{A_e\sqrt{\mu\rho_q}} \tag{2.18}$$

Where $\Delta_f$ is the change in the frequency of the crystal in Hz, $\Delta_m$ is the elastic mass change in grams, $f_0$ is the intrinsic crystal frequency in Hz, A is the area of the electrode in $cm^2$, and $\mu$ and $\rho_q$ are the shear modulus and the density of quartz, these being $2.95*10^{11}dyn/cm^2$ and $2.65g/cm^3$ respectively. If we combine the constants and assume a relatively standard intrinsic crystal frequency of $9MHz$ and a surface area of $0.196cm^2$, we obtain a value for the QCM sensitivity, $C_f$, of approximately $0.903Hz/ng$, from which it is evident how sensitive this instrument can be. Even the addition of a single nanogram is detectable through use of a QCM, though naturally, operating on such small $\Delta_m$

would require careful management of noise and other sources of error.[55]

The Sauerbrey Equation has limitations, however. It is only accurate for the addition of elastic mass to the surface; that is, mass that oscillates with the same frequency as the underlying crystal with no energy loss. Furthermore, its accuracy degrades significantly for an increase in mass greater than approximately 2% of the crystal's original mass.[55]

Water is not typically considered elastic (indeed, it is entirely viscous!), so it may seem questionable whether or not the Sauerbrey equation is necessarily going to accurately reflect its accumulation into the pores of our films. However, White and Schrag theorized that the Sauerbrey Equation could still be applied to nonrigid films which were sufficiently thin.[56] Specifically, they defined a critical limit of the product of the film thickness (d) and $\beta_1$, a parameter based on the shear wavelength of the medium ($\lambda_S$), under which the Sauerbrey formula could still be applied. $\beta_1$ is defined as follows:

$$\beta_1 = \frac{2\pi}{\lambda_S} = \sqrt{\frac{\omega_c \rho}{\eta_M}} cos[\pi/4 - \phi_L/2] \tag{2.19}$$

Where $\omega$ is the radian frequency of the vibrating crystal, $\rho$ is the density of the material, $\eta_M$ is the magnitude of the complex viscosity of the material and $\phi_L$ is the relative phase angle of the liquid medium. In perfectly viscous materials, $\phi_L = 0$ and in perfectly elastic materials, $\phi_L = \pi/2$.

When $\beta_1 > 0.28$, the Sauerbrey Equation can no longer be applied. Thus, so long as our films do not exceed this limit, the Sauerbrey equation will suffice. Vogt et al. found experimentally that this limit was approximately 100 nm for a film of poly(4-ammonium styrenesulfonic acid), a polyeletrolyte.[57]

We can expect that silica NPs, being highly rigid (and thus with very large viscosities), would have a much smaller value of $\beta_1$ compared to the polyelectrolyte film, and consequently the thickness

would need to be significantly larger than 100 nm for us to be at risk of falling outside the Sauerbrey Equation's applicable range. Our films are formed at or below a thickness of 100 nm, thus we can assume the Sauerbrey formula applies.

Similarly, the PEM films being examined here have thicknesses well below 100 nm. The Sauerbrey Equation should thus apply to them with little expected deviation except in their most swelled states.

### 2.4.2 Spin Coating

Alongside dip coating, E-beam evaporation, sputtering and meniscus coating, spin coating is one method by which particle or polymer films are commonly deposited onto rigid and flat or slightly curved substrates.[58, 59] As the name suggests, spin coating is achieved by rapidly spinning a substrate in order to facilitate the formation of the desired film layer. Unlike the other, relatively time consuming methods of film deposition (e-beam can take 10-20 minutes per layer, for example), spin coating can deposit uniform, monomolecular layers in a very short time span, with some publications reporting a deposition rate of 20 seconds per layer at high (5000 rpm) spin speeds.[58]

Spin coating is by definition a batch process. Because each substrate needs to be spun independently from each other substrate, it's impossible to develop a continuous spin-coating method, and compared to roll-to-roll processing, spin coating is relatively inefficient at preparing a large number of films simultaneously. Regardless, the limitations of the process are insignificant at the lab scale; we are interested primarily in the performance of individual films, so mass production is not necessary for this study.

In the ideal case, when materials are spun onto a substrate, the result is a well-ordered, uniform film. However, there are a number of factors that can influence the spin coating process, affecting

properties such as film distribution, thickness and uniformity. These include substrate quality, roughness and hygiene, as well as temperature and airflow conditions both of which can affect the rate of solvent evaporation. Other significant factors include angular velocity, fluid viscosity, solvent-surface interactions. For particle suspensions in particular, important factors also include solvent-particle interactions, particle concentration, particle shape and particle size.[60]

Ensuring substrate quality and cleanliness is a vital step in the spin-coating process. If, for example, the substrate is not properly cleaned prior to the spin coating process, there is a strong possibility that streaks or pinholes of irregularly dispersed material can appear within the resulting film. In general, the receiving substrate must be properly cleaned and prepared prior to undergoing a spin-coating process.

Bornside et al. divided the spin coating process into four stages.[61, 62] Three of these stages (deposition, spin-up, spin-off) occur sequentially, while the fourth (evaporation) takes place over the entire process.

Deposition involves the addition of an excess amount of liquid containing the particulate or polymer which is to comprise the film in solution. This step takes place either prior to initiating the substrate's rotation, or while the substrate is spinning at some initial, constant rate. The solvent containing the material which will form the desired layer is deposited onto the substrate until it completely coats the surface. If the substrate is rotating, the deposition is typically performed at its center, and the coating is formed via centrifugal force. If not, then the substrate must be covered evenly by manual injection before initiating rotation. This step ends once the desired amount of material is delivered to the substrate.

Following this, the spin-off process begins as the substrate begins to spin and a majority of the

solution is drawn towards the substrate's perimeter, whereupon it accumulates and leaves as large droplets. The remaining liquid layer thins substantially during this stage, and resistance to flow rapidly increases with decreasing thickness. Eventually, enough fluid is expelled that the remaining film- often merely nanometers thick- is thin enough that its rotational speed is nearly identical to that of the substrate. At this point, viscous drag force of the remaining material will match and oppose the rotational acceleration. At this point, the loss of bulk fluid (droplets, etc) ends. Solvent is however still lost via evaporation, which begins to increase the concentration of non-volatile components (typically the polymer or particles that will go on to make up the film), thus increasing viscosity as well. At the last stage, spin-up, evaporation fully dominates as the primary mechanism by which liquid is removed from the film.

Once a majority of non-volatiles have been removed, the coating material begins to dry and an elastic or viscoelastic gel film begins to form. In spin-coating, this film formation is driven primarily by the rapid, convection-driven evaporation from the surface. However, even after the spin coating process has completed, capillary pressures still cause further compacting of the film. As the remaining liquid is drawn down through the film comprised of the non-volatile components by evaporation, capillary tension is induced (P) which is in turn counteracted by compressive stresses acting on the non-volatile phase. This results in a denser film, but also poses the risk of cracking.[62]

When a film is fully solidified and can no longer flow across the substrate to which it is attached, any further compression or expansion generates tensile stresses across the two-dimensional surface formed by the film. This may result in failure of the film structure, causing cracks to form. However, it is shown that crack formation can largely be mitigated by maintaining a film thickness beneath a certain critical thickness (0.5-1 $\mu$m).[62] Thus, in order to avoid encountering the obvious optical aberrations that would emerge from trying to scan a cracked films, we attempt to ensure a film

thickness well below this critical limit. While an equation for film thickness as a function of solution viscosity, mass of volatile solvent per unit volume and evaporation rate does exist as modeled by Meyerhofer, the spin coating process used here is quick and simple enough that measurements of film thickness vs spin speed or number of layers is sufficient.[63, 59, 62]

From an economic perspective, the use of spin-coating to produce a large quantity of sensor-components is largely unfeasible. In most cases, spin coating is not especially compatible with particularly large substrates. Deposition of high quality films has been achieved with substrates wafer-sized and smaller, but the substrate size appears to be limited by the effect of rotation on its structural integrity. Larger substrates are more prone to shattering, for example.

The spin coating process is also highly resource intensive. Large quantities of solution are lost, and relatively little of the material initially deposited onto the substrate will remain in the resulting film. Without the use of an expensive recycling system, this seems to be an issue that is inherent to the process itself, and may only be solved by careful engineering of the spin coating system. However, for small-scale laboratory experiments involving the creation of individual samples, these economic factors are relatively insignificant, as usually only very small amounts of material are in use.

### 2.4.3 Important Sensor Terminology

The discussion of sensor design necessitates the use of a particular lexicon. While a full discussion of the myriad definitions and terms associated with sensor technology is unnecessary, there are a handful which are particularly important for the analysis of the two sensors detailed in Chapters 3 and 4. David S. Nyce defines the terms in the glossary of his text as follows:[64]

**Hysteresis:** "The measure of a sensors ability to produce an output indicative of changes in the

input parameter regardless of whether the input is increasing or decreasing." An ideal sensor exhibits no hysteresis, resulting in the same output at a given input regardless of how or in which direction the input data is changing.

**Nonlinearity:** "The maximum deviation between a best straight line drawn through the sensor output data and the actual data points."

**Resolution:** "The smallest change in the measurand that the sensor is able to detect."

**Sensitivity:** "A ratio of the amount of change in output signal resulting from an amount of change in the input measurand."

# 3 SILICA NANOPARTICLE FILM

## 3.1 Introduction

Nanoparticle films have been the subject of much study and experimentation over the past several decades. R.K Iler in 1964 first reported the deposition of single-layer colloidal silica on an alumina surface.[65] He would later go on to develop multilayer films of colloidal particles using a method that we now know as layer-by-layer assembly.[66] Since then, the study of nanoparticle films has expanded to encompass a wide range of fields, from developing biomaterials, to serving as catalysts, though the most relevant applications to this thesis are those involving sensing and the unique optical properties of many nanoparticle films.[67, 68]

## 3.2 Background

A relatively recent paper by Wang in 2005 described the application of a silica nanoparticle aerogel thin film as a resistive humidity sensor.[12] Somewhat earlier, in 2003, Bearzotti and her associates utilized a mesoporous silica film as not only a resistive humidity sensor, but also a sensor for the presence and concentration of alcohol.[69]

While operating under somewhat different principles to the sensors described here, Wang's and Bearzotti's work illustrates the utility of these films as humidity sensing devices. These films are highly porous, possessing a very large surface area for their relatively small volume, which allows them to express impressive sensitivity to changes in ambient vapor compositions.[12] These films can

also exhibit relatively low hysteresis. For instance, Wang and his associates studied the electrical resistance of a silica NP aerogel film with changing humidity. They found that the hysteresis loop exhibited a maximum separation of only 3.3% RH between the humidification and desiccation curves with a minimum humidity of 20%RH, a maximum humidity of 90%RH, and a film pore size of approximately 20 nm. They also observed a change of almost 0.4 $M\Omega$ over this range.

Similarly, Bearzotti studied the electric current intensity of a silica film over a range of 5 to 95 %RH. They observed an increase of current intensity of almost five orders of magnitude (Units of Amps) and found that the response possessed only a very small hysteresis loop.[69]

In general, however, the methods utilized by these two groups to prepare the sensing surface are somewhat involved, requiring several steps and the use of organic molecules to provide a template for the construction of the nanoparticle film. There are a number of methods by which a nanoparticle film may be deposited, including electrodeposition, the Langmuir-Blodgett method, sol-gel and multilayer assembly.[70, 71, 72, 73, 74, 75, 76, 77]

Of the many that are available, among the simplest and most practical is deposition via a single-step spin-coating method, as presented by Cook et al. in 2012.[18] This method involves the preparation of a precursor solution of 12 nm LUDOX SiO2 NPs by pH adjustment, aging and dilution before performing a simple single-layer deposition. This treatment was originally devised in order to produce quarter-wave antireflection coatings, but Cook et al. found that the effective refractive index of the films would vary with changes in the relative humidity of the environment. This finding would lead directly to the investigation of the optical response of these films to ambient humidity, which eventually culminated in this thesis. A more detailed description of this technique can be found in the Methods section.

This method is capable of producing films with highly tunable and predictable thicknesses and refractive indices, which is appealing for application as an optical sensor. Cook et al. found that by simply varying the amount of time spent in the precursor aging step as well as the aging temperature, both the coating thickness (and by extension, the coating density) and refractive index can easily be controlled.

Specifically, they found that, for a constant spin speed, the thickness of a film could be increased from around 70 nm to 140 nm simply by aging the precursor for an hour at $60°C$. Comparatively, it took almost 48 hours for a solution aged at room temperature to reach comparative thickness. Interestingly, regardless of the temperature at which the aging step was performed, the relationship between time and film thickness is approximately linear.

Refractive index was observe to decrease with increasing film thickness before eventually reaching an asymptote region at approximately n = 1.25 and a thickness of 120 nm. Porosity was observed via SEM to increase significantly with increasing film thickness as well.

The films produced with this method are highly porous due to the agglomeration that occurs when the solution pH is dropped to near-neutral. As the nanoparticles grow, the films they form tend to be less dense and possess much greater void fraction than that of an unmodified solution. This was first utilized in order to develop antireflection coatings with more air-like refractive indexes (i.e. $n_{air} = 1.00$), but could also make the films more sensitive to the effects of local humidity due to the increase in the volume fraction occupied by pores.

It is necessary, however, to determine that changes in the refractive index are indeed due to a humidity response and not the result of some structural change or addition of water only to the surface of the film. In order to do so, we first need a method by which water can effectively be prevented

from entering the porous network without otherwise substantially altering the film nanostructure. Secondly, we require a means to independently measure changes in the films that could be the result of the bulk addition of water to the system. As the films take up water, displacing the air within, we would expect them to increase in mass, which makes a mass measurement convenient. However, due to the very small volumes involved in the process, any such measurement would need to be extremely sensitive to changes in mass.

Fortunately, there are well-known and widely used methods to accomplish both tasks. The method chosen to prevent water infiltration is the complexation of a silane onto the silica surface. Silanes are widely used to modify surfaces for hydrophobicity, and could prevent the infiltration of water into the film's porous network.[78, 79, 80, 81, 82] If the refractive index is indeed responding to ambient humidity, then the addition of a silane should prevent any changes from taking place. The change in the hydrophobicity of the surface can be measured easily through the use of a drop-shape analyzer. The higher the contact angle, the more hydrophobic the surface becomes.

The second task can be accomplished through the use of a quartz crystal microbalance, or QCM. The QCM operates by monitoring the oscillatory frequency of a quartz crystal under an alternating electric field. Any decrease in that frequency can be interpreted as an increase in the mass of a sample. Thus, in order to verify that any observed change in optical properties are indeed due to a change in the water content of the film, we need to prepare samples of silica film for optical testing as well as mass testing.

Once the control tests have been performed, both films can then be treated with the silane and tested with contact angle measurement in order to evaluate whether the treatment was indeed successful in inducing hydrophobicity. If so, then the optical and mass tests can be repeated and the results compared. There is naturally a risk that the silane treatment might damage or degrade the

films during this step, but refractive index measurements suggested that any changes to their physical structure is negligible.

### 3.2.1 Silanes

Molecular silane is of rather familiar chemistry and is comprised of a single silicon atom bonded to four hydrogens, i.e. $SiH_4$. The group of compounds derived from this basic structure is far more diverse, and together form the foundations of silicon chemistry. The silanes are characterized as saturated molecules consisting of at least a single silicon group, and may be capped or terminated by a wide variety of functional groups. These groups are highly tunable, and include amino acids, halogens, simple organic molecules and a wide variety of other substances. This flexibility and tuneability allow the silanes to rival the versatility of their close relatives, the alkanes. This, coupled with their relatively low cost, has led to wide application to surface chemistry, silicon chemistry and other fields.[78, 79, 80, 81, 82]

One particular subgroup within this family of molecules are the organochlorosilanes, whose substituent groups consist of one or more organic moieties and at least one chlorine atom. This group is particularly useful for surface chemistry, as it's well known that organochlorosilanes can react with the hydroxyl groups on the surface of silica, resulting in the formation of a siloxane (Si-O-Si) linkage. The remaining functional groups, which for our purposes are made up of a single long-chain hydrocarbon, can thus be coupled to an appropriate surface, which can have dramatic effects on the surfaces properties.[83, 84, 85]

In this case, the silane-hydroxyl reaction delivers a long, organic functional group to the silica surface, thus forming a highly hydrophobic, yet extremely thin layer. In some cases, this organochlorosilane reaction can form an extensive network of linked silanes, depending on the silane chosen.[79]

A chlorosilane with multiple chlorine groups may undergo crosslinking, producing a thick organic layer which may actually change the effective refractive index of the film.[86] As such, an organochlorosilane with a single chlorine group would be ideal; such a molecule would still be able to form a hydrophobic layer, obstructing the infiltration of water into the porous network, without significantly affecting the refractive index of the films. To this end, chloro(dimethyl)octylsilane was chosen, which was found to produce a highly hydrophobic coating to little to no detriment of the films original optical properties. The chemical structure of the silane molecule and chlorosilanes can be seen in Figure 3.1. A simple diagram describing the difference in surface chemistry occurring with the use of a monochlorosilane and trichlorosilane can be seen in Figure 3.2.

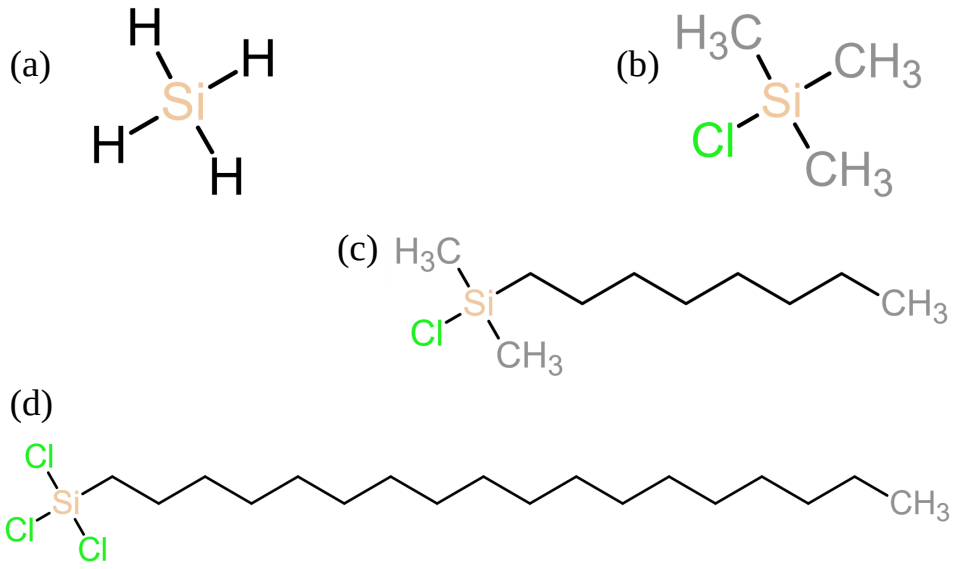


Figure 3.1: Chemical structures of (a) Molecular Silane; (b) Chlorotrimethylsilane; (c) chloro-(dimethyl)octylsilane; (d) trichlorooctadecylsilane

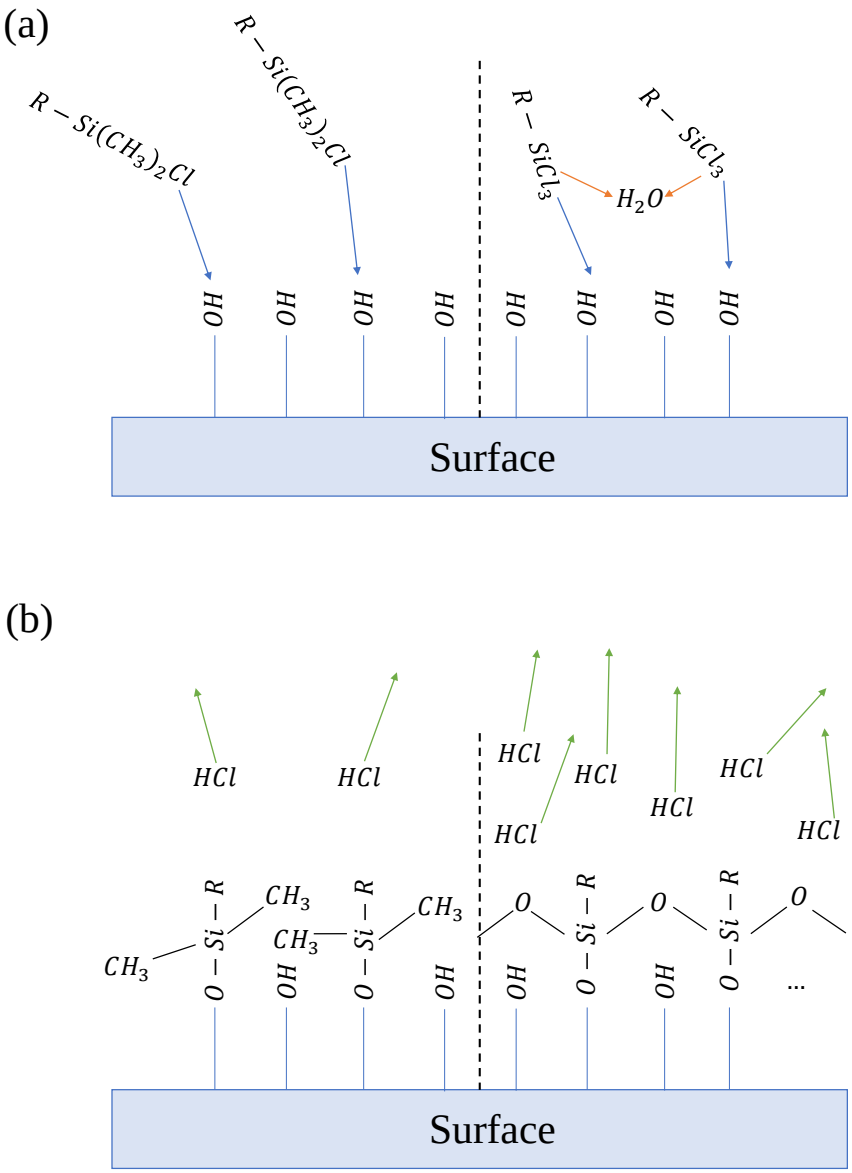


Figure 3.2: Diagram of sample surface reactions with monochloro (left) and trichloro (right) silanes. (a) and (b) depict the silica surface before and after reaction of chlorosilanes with with surface hydroxide groups.

## 3.3 Methods

### 3.3.1 Sample Preparation

Sample preparation was performed in accordance to the method described by Cook et al. and duplicated in summary form here.[18] A silica precursor was prepared from Ludox HS-30, 12 nm diameter solution obtained from Sigma Aldrich. The pH of an aliquot of approximately 5 mL was adjusted to around 6.5 by the dropwise addition of 1 M hydrochloric acid (HCl). Once brought down to this near-neutral pH, the nanoparticles will readily begin to agglomerate and form clusters. In order to facilitate aggregation, the sample was placed into an oven and heated to 60$^o$C for approximately one hour, or until the precursor takes on a honey-like consistency. In order to assure consistent bulk agglomeration rate, the sample was turned over twice every fifteen minutes.

Once heated for a sufficient span of time, the aliquot was diluted to 5% by weight with 18 $M\Omega$ Ultrapure Water, which also served to quench the reaction. The solution may then by spin-deposited onto substrates as needed. For the optical portion of these experiments, a silicon wafer was chosen as the substrate. While glass slides were considered as a possibility, it was decided that depositing a silica film onto a silica substrate would not produce particularly useful results due to the highly similar optical properties of the film and the bulk glass. The QCM tests, however, necessitated the use of an only slightly more complex substrate.

The gold-chrome disks used in the QCM tests are highly hydrophobic. As such, it became necessary to first deposit a 0.5wt% polystyrene film onto the surface of the disk. This was done via spin-deposition at 8000 RPM, which was found to produce a film that was both robust enough to support the silica layer, and thin enough at 4.77 nm as to minimize its effect on the experimen-

tal results. Unmodified polystyrene is still highly hydrophobic, but exposing the film to UV-Ozone causes the formation of hydroxyl and carboxyl groups on its surface.[87] This drastically reduces the hydrophobicity of the film, and allowed us to spin-deposit the silica as normal.

For the purposes of our experiments, intervals of 1000 RPM from 2000 to 8000 RPM were chosen as the spin deposition speed.

### 3.3.2 Ellipsometry

Ellipsometric tests were performed using a J.A. Woollam alpha-SE ellipsometer and associated CompleteEASE software. Samples prepared through the method described above were placed within an enclosed humidity cell designed with Solid Edge modelling software and produced through use of a 3D printer. A diagram of the cell from four angles can be found in Figure 3.3. These cells were enclosed by a combination of polymer wrap and long glass cover-slips of approximately 0.17 mm in thickness, chosen to provide a transparent window for the transmission of the light beam while minimizing said windows influence on the resulting data. The window was set at an angle of 70 degrees in order to match the angle of measurement typically used for collecting ellipsometric data. This would ensure that the inclement light probe would arrive at the glass at a perpendicular angle, minimizing its effect on the measurement.

Humidity was controlled via the use of saturated salt solutions. It's well known that saturated salt solutions are capable of regulating the humidity within small, enclosed space, and indeed these binary salts are often used to calibrate hygrometers in industry.[88] Lithium chloride was used to approximate dry conditions ($\phi_{LiCl} = 11.30\%$) while potassium sulfate was used to approximate humid conditions ($\phi_{K_2SO_4} = 98.0\%$).[88]

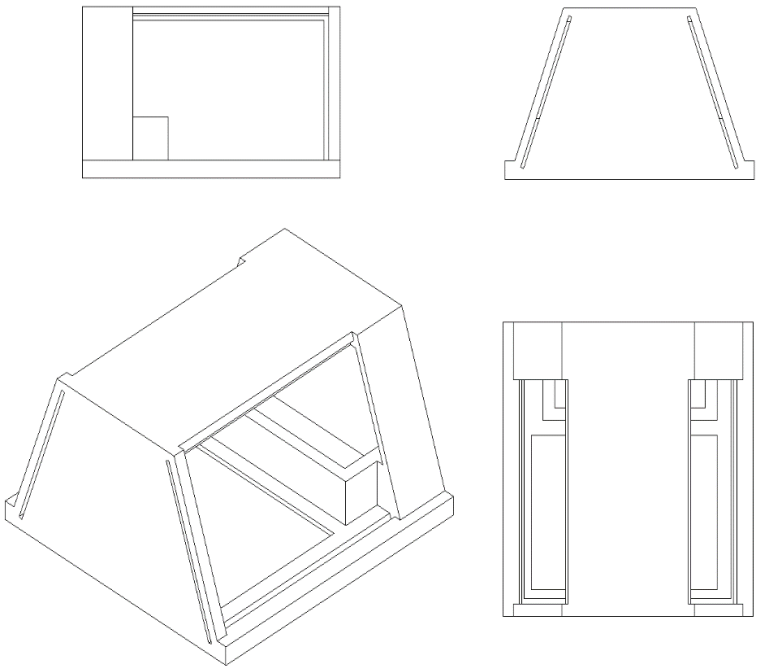

Figure 3.3: Diagram of humidity cell from four angles.

Prior to performing any humidity trials, the sample was placed into the humidity cell at room conditions and set in the center of the ellipsometer's measurement stage. The ellipsometer was then moved to its 70 degree contact angle setting and an initial measurement was performed. The ellipsometer's measurement stage was then shifted manually until its light beam seemed nearly aligned to the optical sensor. It was then set to automatically adjust the measurement stage's elevation in order to achieve the best possible position for measurement.

Once the initial position calibration was completed, the sample was removed from the humidity cell and one of the salt solutions was placed within a small trough built into the cell's interior by disposable dropper pipette. After ensuring no solution had splashed out of the trough, the sample was placed into the depression at the humidity cell's center. The glass cover slip was then moved back into position.

Upon sealing the humidity cell, the samples were interrogated by the ellipsometer at a contact angle of 70 degrees using its fast data acquisition mode. In the first measurement, the stage was again allowed to shift to accommodate for any changes that might have occurred during the sample loading phase. All subsequent measurements were taken at the same vertical position at intervals of 3 second in order to capture as much of the transient behavior of the system as possible. The room humidity was monitored throughout the tests, and was estimated to be at approximately 44% for the duration of the experiments.

The resulting optical profiles were fitted to obtain data on the apparent film porosity by use of a simple, two-component Bruggeman EMA model comprised of silica (material 1, $n_c = 1.462$) and void (material 2, $n_d = 1$) which here represents air on a silicon wafer substrate. From these models, we were able to extract the approximate void fraction of the films, the refractive index of the mixed material at $\lambda = 632.8nm$ and the film thickness.

### 3.3.3 Glovebox Specifications

The glovebox used in the QCM experiments and elsewhere in this thesis was made of acryllic glass with dimensions of approximately 18"/24"/36" in depth, height and length. The glovebox was equipped with a pair of built-in rubber gloves on one of its wide faces. Opposite was an electric heater with built-in auxillary power outlets and an electric fan to facilitate the thorough mixing of air within the system. A supplementary fan and cooling system were also present in case tighter control was necessary.

The door was located on the operator's left hand side and sealed with a rubber gasket to ensure containment. Small cable ports also on the left hand side were used to feed instrument power supplies, sensor feeds and so on into the box. Polymer laboratory wrap was used to cover these ports and

accommodate the instrument cables in order to maintain as tight of a seal as possible when in use.

Also along this bank of ports were a pair of specially designed inlets. One of these was attached to a commercially purchased electrical humidifier. The second was used to supply desiccated campus air to the chamber through an electronically controlled solenoid valve.

Control over the conditions within the glove box was achieved through the use of a Cole-Parmer Electrotech Systems Digital Humidity PID controller with Temperature display. The power supply for the humidifier and solenoid valve were routed through this controller which automatically maintained humidity conditions within 1.5 %RH of the set-point. Temperature was controlled through the use of a seperate PID, through which the power supply of the heater and peltier-type cooler were routed. For both instruments, temperature and humidity sensors were placed inside the chamber to monitor its conditions.

During experiments, the required instruments were placed into the glovebox and their electronics fed through one of the available side-ports. Care was taken to ensure that any breach of the closed environment was minimized, and only the required instruments were utilized at any given time.

### 3.3.4 QCM Tests

All QCM experiments were performed using a Stanford Research Systems 5 MHz QCM200 and its associated software package. This unit utilizes a 5 MHz, 1" diameter, AT-cut crystal quartz wafer with circular, gold chrome electrodes on both sides as its sample analysis platform. The instrument has a resistance range from 0 to 5000 Ω and variable resolution between 0.001 to 0.1 Ω depending on the chosen measurement range. In this case, the total change in resistance and total measured resistance were both well under 100 Ω, with the latter being around 10 Ω in total. This places our

measurements well within the $0 > R > 100\ \Omega$ range, with a resolution of $0.001\ \Omega$.

The sample preparation was specified in the relevant section above. Once deposited onto the QCM disk, the sample was loaded into the sample analysis platform and placed within a sealed, environmental-control glove-box.

The pipe-shaped measurement arm was placed such that it extended through one of the available ports on the glove box into the test chamber itself. This was done only because it was found that exposure to high humidity caused permanent damage to the electronics built into the sample analysis platform. As a precautionary measure, it was necessary to ensure that the electronic components remained outside the chamber. However, to ensure that the humidity readings matched the changes in mass, the PID's humidity sensor was placed close to the sample and the sample itself was inserted as far as possible into the humidity control chamber. The environmentally sealed environment was ensured through the use of polymer wrap pulled taut around the ports in use.

Using the PID humidity controller, the humidity was initially set to 10% RH and the system was allowed to equilibriate over the course of ten minutes. Once equilibriated, the QCM200 software was used to begin collecting data.

An initial period of around 90 seconds was alloted in order to measure a baseline response at 10% RH. Following this, the humidity set point was moved to 90% RH and the system was allowed to reach equilibrium, a process which took approximately a minute. Once the mass readings likewise reached steady-state, the system was set to hold 90% humidity for another five minutes before the set point was moved back to to 10% RH, taking approximately one minute to achieve. The system continued to collect data for another five minutes to attain another set point and ensure a new steady-state was reached. Temperature was held constant throughout this experiment at $25^oC$.

## 3.4 Results and Discussion

### 3.4.1 Evaluation on Effects of Spin Speed on Film Thickness

In order to test the effect of deposition conditions on film structure and optical properties, a short test was performed to evaluate the effect that spin speed (in RPM) had on thickness and refractive index for a particular pair of precursors which were prepared identically to evaluate repeatability. The results have been collated into Figure 3.4.

As was expected from the review of spin coating methods, there is a slight decline in the thickness of the film to approximately 60 nm with an increase in spin speed.

For the agglomeration method used in this experiment, DLS data from Cook et al.[18] predicts a growth mechanism of first-order kinetics:

$$D = D_o exp(Ct) \tag{3.1}$$

Where C is a particle growth rate constant, D is particle hydrodynamic diameter and $D_o$ is the original particle hydrodynamic diameter before growth. For a temperature of 60$^o$C, we predict a particle growth rate constant of approximately 0.25, which for a 12 nm silica NP precursor solution allowed to age for an hour results in a average agglomerate size of approximately 16 nm in diamater.

This implies that the prepared films are multiple layers thick; assuming that the agglomerates are approximately spherical and more or less close-packed, we can estimate the height of the structure. With a three dimensional coordinate system, x, y, z, the midpoint height or y coordinate of the first row of spheres is equal to the radius r. With the closed-packing assumption, each sphere in each

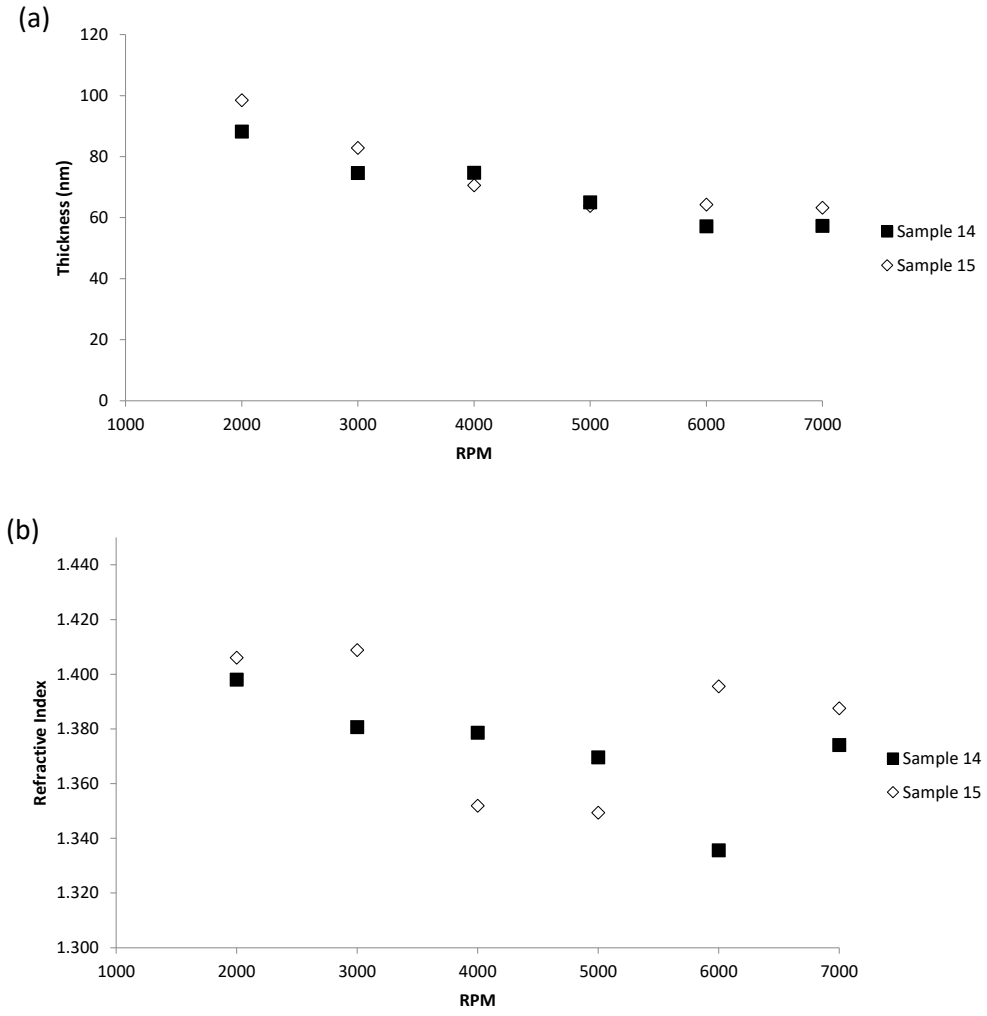


Figure 3.4: Graphs of: a) Thickness VS Spin Speed for Two Sample Precursors; b) Refractive Index VS Spin Speed for Two Identically Prepared Sample Precursors

additional layer has a y coordinate of $r + (n-1)\sqrt{3}r$ where n is how many layers from the substrate surface the sphere belongs. The height of the very top of the film, adds one more radius, to a total thickness (h) of $r + (n-1)\sqrt{3}r = h$

We can see then that the number of layers in the film seem to range from either approximately 7 (corresponding to a thickness of 100 nm) to 4 (corresponding to a thickness of 60 nm).

It is possible that, rather than stripping layers, reduction of film thickness is the result of additional deformation of the nanoparticle agglomerate clusters or an increase in the film stack density. The effective material refractive index is tied to the fraction of void space in the films. Thus, one would predict that any increase in film density, which would likely be attributed to a reduction of porosity, would result in an increase in the refractive index. As seen in Figure 3.4b, increasing spin speed or decreasing thickness does not appear to have any effect on the refractive index of the films. The spread is apparently random for films produced with either precursor, with an average refractive index of approximately n = 1.380 for both regardless of spin speed. This seems to indicate that spin speed does not significantly affect the porosity of the films. Thus, any change of thickness with increasing spin speed would appear to be the result of layer losses. This evidence is hardly direct, however, and additional investigation is necessary to evaluate the exact effect spin speed might have on the film morphology. These experiments could perhaps be performed via transmission electron microscopy, but such tests are beyond the scope of this thesis.

It is interesting that the thickness appears to reach an asymptote at high spin speeds. However, Rehg showed that for a substrate that accelerated at a constant rate as opposed to an instantaneous acceleration to some final spin speed, the thickness would tend to reach an asymptote at high rotational velocities.[60] When acceleration is finite and constant, the film reaches its final thickness while the substrate is still accelerating. Recalling the regimes that make up the spin coating process, this

essentially means that a majority of the solvent has wicked off by the time the substrate has reached its maximum acceleration; the spin-off mode has passed, and any additional matter being ejected is minimal.

### 3.4.2 Optical Response to Humidity and the Effect of the Silane

Based on the difference in thickness between films produced under different spin rates, it is of interest to evaluate the behavior of a relatively thicker film compared to that of a relatively thinner film. The reason is twofold. First is to evaluate whether one is more responsive than the other, the second is to determine whether moisture is indeed taken up by the entire film or if it's simply a surface effect. In both cases, humidity was controlled through the use of oversaturated salt solutions of $LiCl$ and $K_2SO_4$. The films were then treated with silane as described in the methods section and the tests were repeated. Ellipsometric results of these tests can be found in Figures 3.5 and 3.6, representing experiments with films spun at 2000 and 7000 RPM respectively.

The graphs indicate some interesting results; as can be seen in 3.5 and 3.6 c and d, the initial measured void fraction is consistent and equal between the two films. Regardless of the rotational velocity associated with their deposition, the films appear to have similar porosity, which seems to indicate that void space is independent of deposition speed. Moreover, changes in humidity appear to be directly responsible for the change in refractive index. Variation occurred only upon exposure of unmodified to high/low humidity environments.

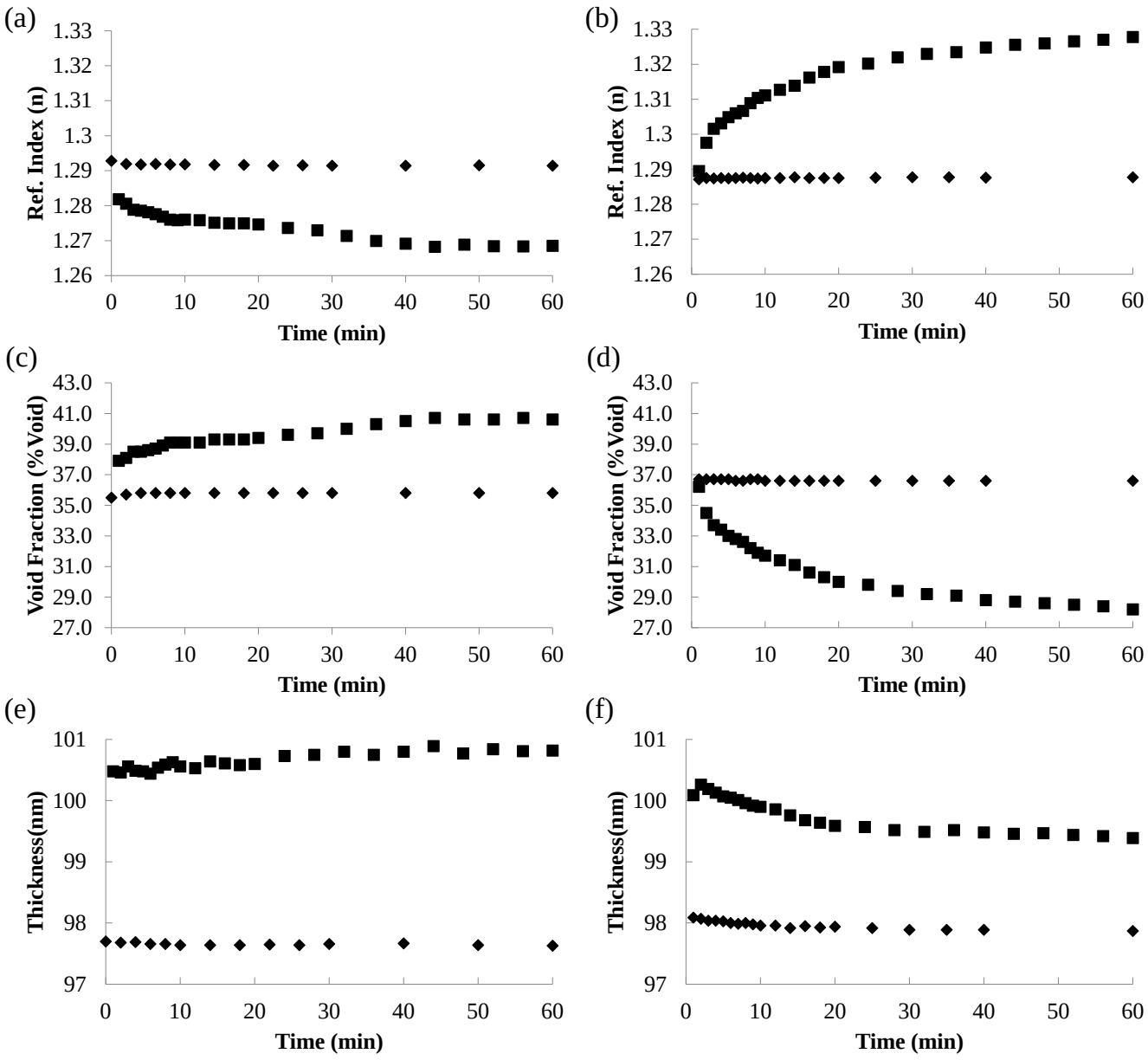


Figure 3.5: Ellipsometry Results of 2000 RPM Spun Film. Left-hand figures denote behavior in dry environment. Right-hand figures denote behavior in humid environment. (a,b): Refractive Index, (c,d): Void Fraction, (e,f): Thickness. Squares: Untreated NPs, Diamonds: After Silane Treatment

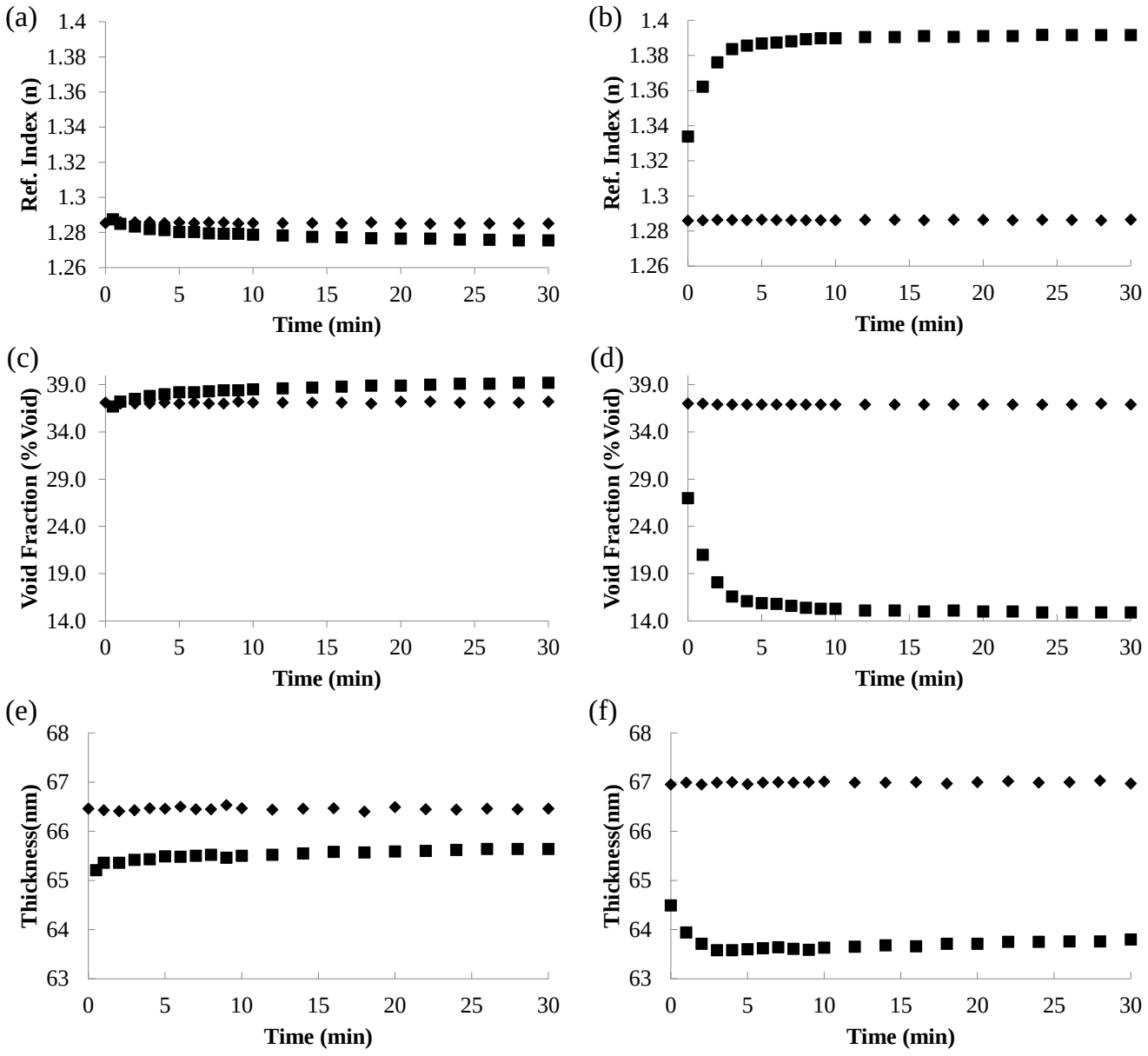


Figure 3.6: Graphs of Ellipsometry Results of 7000 RPM Spun Film. Left-hand figures denote behavior in dry environment. Right-hand figures denote behavior in humid environment. (a,b): Refractive Index, (c,d): Void Fraction, (e,f): Thickness. Squares: Untreated NPs, Diamonds: After Silane Treatment.

Reaction with silane successfully rendered the surface superhydrophobic (see Fig. 3.7) and completely prevented any change in optical properties under changing humidity conditions. It also evidently did this without altering the structure of the films outside of the addition of hydrocarbon groups to the silica surface, as seen in Table 3.1. This evidence indicates that the uptake of water played a significant role in the films' changing optical properties. Furthermore, the fact that the film survived submersion in the reaction solution with only negligible changes to its structure is additional evidence as to its robustness.

However, there does appear to be some time-dependent behavior. The films require a period of several minutes for their optical properties to achieve steady state. Due to the method by which humidity was controlled, it's difficult to determine whether the time-dependent behavior is due to transport of water vapor through the environment enclosed by the humidity cell or due to the adsorption/uptake capabilities of the film stack itself. It is possible that the film is in fact extremely responsive and that the timescale associated with the adsorption process is much shorter than the time required for the change in salt solution to adjust the local humidity. It's also possible that the seal devised for the humidity cell was insufficient in controlling the transport of water vapor into and out of the cell, which would potentially explain the difference in the behavior of the films upon exposure to high humidity. One may simply have equilibriated at a lower humidity than the other due to a difference in the rate of transport of water vapor into and out of the cell which might have resulted from imperfect sealing conditions, different ambient temperatures and so on.

We can estimate a time constant for the apparent first order kinetics of the optical response by approximating the time at which the film's refractive index has reached $1 - 1/e$ or approximately 63.2% of its final equilibrium value.[89, 90, 91] The results have been compiled in Table 3.2 below.

Table 3.1: Summary of Optical Properties and Relevant Film Qualities Prior to and Following Silane Treatment.

| RPM | Silane | Void Fraction (%) | Ref. Index (n) | Thickness (nm) |
|---|---|---|---|---|
| 7000 | No | 37.2 | 1.2851 | 66.46 |
| 7000 | Yes | 39.2 | 1.2755 | 65.64 |
| 2000 | No | 35.9 | 1.291 | 99.63 |
| 2000 | Yes | 35.1 | 1.2947 | 97.66 |

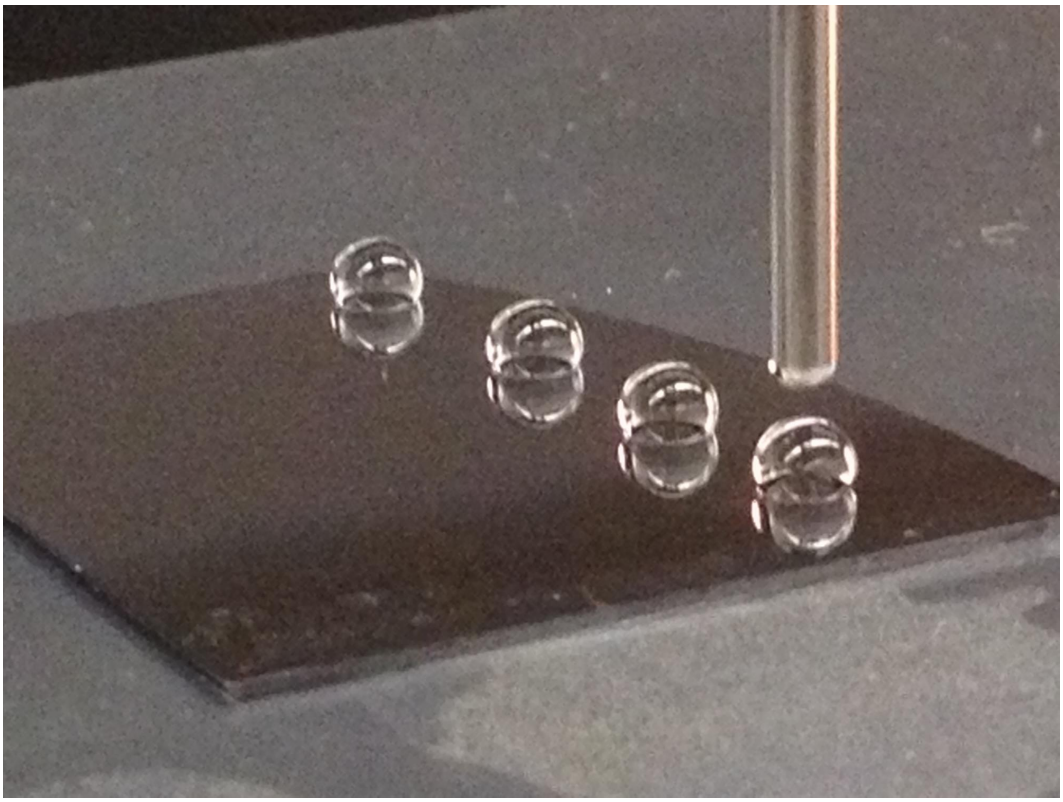

Figure 3.7: Evidence of superhydrophobicity of silanized silica NP film. Note highly spherical water droplet formation.

Table 3.2: Summary of the Time Constants for the First Order Kinetics of the Refractive Index Response to Humidity.

| RPM | Salt | Time Constant (sec) | Ref. Index (n) |
|---|---|---|---|
| 7000 | $K_2SO_4$ | 90 | 1.3691 |
| 7000 | LiCl | 300 | 1.2802 |
| 2000 | $K_2SO_4$ | 840 | 1.3139 |
| 2000 | LiCl | 1560 | 1.2734 |

These time constants are very clearly on the order of minutes. Pinnes defined that the time constant associated with the first-order diffusion of water vapor through a membrane film of thickness L and diffusivity D into a relatively small airspace was equal to $0.48L^2/D$ with units of seconds.[90] If we consider the 100 nm films above to be particularly porous membranes with relatively high diffusivities, we expect the time constant to be very small indeed.

For example, H. Park studied a porous polyethylene-terepththalate (PET) film in which water vapor was found to have a diffusivity of around 1.25E-5 $m^2/s$.[91] Assuming in the worst case that the films have a diffusivity equal to only 1% of this (or 1.25E-7 $m^2/s$, then the time constant associated with a 100 nm film would still equal 8.0E-10 seconds. The time constants associated with the graphs is on the order of hundreds of seconds, a dozen orders of magnitude larger than these calculated values. It seems reasonable to conclude that the time-dependent behavior observed in Figures 3.5 and 3.6 is likely associated with the diffusion of water vapor from the surface of the saturated salt solution into the air space of the humidity cell.

The comparatively large change in refractive index of the 7000 RPM film can be explained either due to a flaw in the experimental apparatus or to the relative thinness of the film itself. It could be that moisture is unable to completely permeate the thicker, 2000 RPM film, which would explain why the refractive index is observed to be less sensitive to changes in humidity. This may also indicate a non-uniform uptake of moisture into the nanoparticle lattice, though aside from attempting a prediction

from first-principles, it is difficult to imagine a method of evaluating whether or not this is true.

Swelling and deswelling as indicated by figures 3.5 and 3.6 (e) and (f) is incredibly minor so as to be negligible. Changes over extended periods of exposure to higher or lower humidity is limited to fractions of a nanometer. Thus any water vapor adsorbing onto the film appears to be limited only to filling available void space rather than inducing any structural changes to the nanostructure. No investigation was performed on attempting extended humidifying/dehumidifying cycles, but based on the virtually nonexistent change in the overall thickness of the film, it's unlikely that any long-term changes would take place.

### 3.4.3 Evaluation of QCM Data

Proof for the uptake of water into the silica NP film can be seen in figure 3.8. This data was acquired during a humidity sweep from 10% to and from 90% RH. As can be seen, the untreated film exhibits a considerable increase in the amount of mass gained compared to that of the silane-treated film. Comparing the results to that of the ellipsometric tests, this seems to reinforce the hypothesis that the change in humidity is directly affecting the optical properties of the film by inducing the adsorption of water molecules into the film stack.

Notably, this graph also seems to suggest that, for most practical situations wherein one would normally expect changes in humidity to be relatively gradual and continuous over a period of time, the film response time is adequate. While no graphs are available, the glove box within which the experiments were performed was in fact large enough that the change from 10% to 90% humidity was relatively gradual and occurred over the course of approximately 90 seconds. As can be seen on the graph, the film mass began to increase sharply at approximately 80 seconds, before reaching a constant, if oscillating peak at approximately 170 seconds.

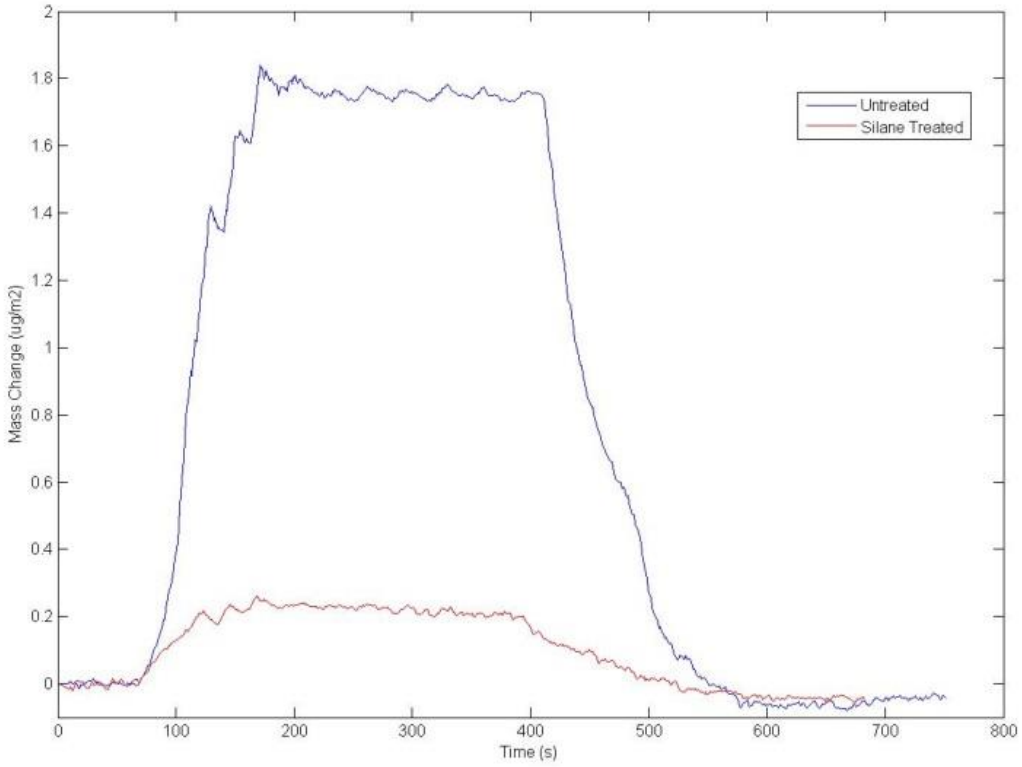


Figure 3.8: Results of treated and untreated QCM tests at 2000 RPM deposition speed

It may seem at first difficult to then say what the source of the oscillations might be, but consider this: The humidity conditions within the glove box were controlled by a PID system. When first set to 90% humidity, the humidifier would switch on and remain in an on state until the relative humidity began to reach the final set point. From here, the PID controller would begin oscillating the up-time of the humidifier and applying regular bursts of desiccated air to control the humidity rise.

This behavior can be seen in the three local maxima prior to the graph's true plateau region. Typically, the PID would allow the glove box to rise to a certain humidity level, then feather the dry air valve until it could properly control the next stage in the climb. It also had a tendency to overshoot the set-point before falling back into a constant, oscillatory pattern– one which is captured in the oscillatory behavior at at the plateau. This indicates that the silica NP film is capable of capturing and releasing moisture at a rate nearly synchronous to that of the changes in the surrounding environment. In other words, the silica NP film not only possesses adequate sensitivity, but also very impressive resolution. Based on this evidence, it's likely that the time-dependent behavior noted in the previous section is largely due to the time required for the conditions inside the humidity cell to reach equilibrium.

## 3.5 Conclusions

We have shown that the optical properties of silica NP films produced by the spin-coating of an intentionally aged precursor respond rapidly to changes in ambient humidity. The effective medium model is capable of taking into account changes in the water content of the films, which can be easily interpreted through analyzing a shift in the apparent refractive index. In order to verify that the observed effects were indeed due to the uptake of water, analysis was performed through the use of the QCM, which clearly indicated a mass change under different humidity conditions that could only

be possible due to the adsorption of water onto the silica surface. This was further corroborated by the addition of monofunctional silane, which not only caused the films to become highly hydrophobic, but also dramatically reduced if not entirely eliminated the sensitivity of the films to changing humidity. All in all, the porous silica film seems to be a very viable platform for continuing research in affordable optical humidity sensors. However the results are not perfect; more work could be done on improving the design of the ellipsometry cell in order to eliminate issues associated with the tightness of the air seal, and it would be interesting to evaluate how the sensitivity of the device might be improved, or whether the silane treatment might be modified to preferentially bind with other chemicals in order to build a customizable, specific sensor chip.

# 4 SILVER NANOPARTICLE-INFUSED POLYELECTROLYTE FILM

## 4.1 Introduction

The application of polymer-metal nanoparticle composite films in developing low-cost humidity sensors has been studied previously my Luechinger et al. in their work on a carbon-coated copper nanoparticle system which utilized colorimetry and SPR in tandem. The latter property is well studied as an effective method to detect changes in the local chemical environment.[41, 92, 93, 94, 95]

The use of SPR in sensing is well studied but typically utilizes a single layer of metal in tandem with the use of a waveguide, grating couplers or other similar surface layers. Gold and silver are commonly utilized in SPR for their strong resonance in the visible and infra-red wavelengths.[95, 96, 97, 98, 99] However, these and other metals which exhibit SPR are relatively precious, especially so for those such as platinum and palladium. Thus it is ideal, in order to minimize costs, to develop a new, more affordable sensor design.

The sensor described in this study is, as previously mentioned, composed of a spin-coated multi-layered film of PAH and PAA. Silver nanoparticles are then grown in this film via impregnation with silver acetate and exposure to UV light, thus resulting in a relatively simple, three-step production method that could potentially be scaled for more intense production.

## 4.2 Background

### 4.2.1 Polyelectrolyte Multilayer Films

A polyelectrolyte is by definition a polymer whose repeat unit contains one or more electrolytic, or charged group. The first comprehensive description of polyelectrolyte multilayer (PEM) films was performed by Decher and his colleagues in 1992.[100] They described a process by which ultrathin organic films could be built by sequentially depositing alternating layers of cationic and anionic polyelectrolytes on a charged substrate.[100, 101, 102, 103, 104]

Take for example a substrate of $SiO_2$ which has negative surface charge as a result of the dissociation of terminal silanols, the deposition of a PEM film would begin by the deposition and adsorption of a cationic layer. We can choose PAH as the cation for this example, which conveniently lines up with the construction of the PEM in our experiments. By depositing a cationic polymer, we have effectively flipped the sign of the surface charge from positive to negative. We can then deposit an anionic polyelectrolyte (PAA is another convenient example) which will then be attracted to the positively charged surface and create a new, negatively charged layer. This process is repeated several times until a film with some desired stack composition has been constructed on our glass substrate.

The PEM films that arise from this method of layer-by-layer construction have a number of very useful features. They boast high sensitivity to a number of different chemical environments, and indeed, sensing has been one of the most promising applications of this technology in industry. However, two properties are more applicable above all others to this study. The first is the ability of the PEM film to swell and deswell under the influence of ambient humidity; a number of studies already exist applying PEM films as humidity sensors for good reason.[101, 17] The second, however, is a peculiar

capability of these films to uptake metal salts, which can then be reduced to form metal nanoparticles. As one might recall, silver nanoparticles have a particularly useful application as SPR-based transducers, transforming information about the dielectric constant of their immediate surroundings into a sensible SPR excitation wavelength.

This second property is less immediately obvious than the first; after all, like-dissolves-like is a fundamental heuristic in chemistry. The charged, polar nature of the polyelectrolyte film enables hydrogen bonding interactions that make it very attractive to water molecules. On the other hand, understanding how PEM films can be used as nanoreactors for the formation of silver nanoparticles requires some brief explanation.

Wang et al. found that, in a PEM film composed of alternating layers of PAH and PAA (conveniently identical to the regime described here), could uptake silver ions in aqueous solution.[101] PAA, or Poly-Acrylic Acid, contains a number of carboxylic acid groups. Free, positively charged silver ions in solution can substitute onto these carboxyl groups in exchange for "free" acid protons, which then enter solution. Once bound to the polyanion, the silver ions can be reduced (for example, by using UV light) to produce nanoparticles embedded in the polyelectrolyte network. It is necessary, however, to carefully control the pH of the films during this process. While it's advantageous to have partial ionization of the PEM, bringing the pH so high as to completely ionize it results in a lack of acid protons for the metal cations to substitute, which in turn forms smaller nanoparticles and results in lower metal volume fractions in the film. This is one reason why the pH of the films in this work have been maintained at approximately 4.0.

### 4.2.2 Surface Plasmon Resonance

Surface Plasmon Resonance or SPR is a phenomenon that occurs when light incident to a metal object with at least one dimension shorter than the wavelength of an impinging beam of light. When this occurs, a time-varying electric field ($E_o$) associated with the light excites electrons in the conduction band of the metal substrate. These electrons then begin to oscillate, reaching a zenith at a certain excitation frequency ($\omega$). The photons responsible for the absorption at or near this excitation frequency are essentially absorbed by these electrons, transforming into plasmons. Thus, when one shines white light on a material with a SPR excitation frequency corresponding to blue light, what we observe with our naked eye would be that the material appears orange– exhibiting an absence of blue, reflected light. For nanowires or nanometer-thickness two-dimensional sheets, the plasmon that is generated is called a propagated surface plasmon (PSP), wherein $E_o$ is not uniform across the structure and other factors such as morphology play a role in determining the wavelength of the PSP mode. For one-dimensional nanoscale objects such as nanospheres, however, $E_o$ is uniform and the dimensionality of the structure becomes less significant. Thus we can reduce the behavior of this so-called localized surface plasmon resonance (LSPR) to a formula dependent on the real ($\epsilon_r$) and imaginary ($\epsilon_i$) components of the dielectric function ($\epsilon$). These components themselves vary based on the excitation wavelength ($\lambda_{exc}$) of the material. It also depends on the extinction cross section ($C_{ext}$), the radius (R) of the nanoparticle and the relative dielectric constant of the material surrounding the nanosphere ($\epsilon_m$).

$$C_{ext} = \frac{24\pi^2 R^3 \epsilon_m^{3/2}}{\lambda_{exc}} [\frac{\epsilon_i}{(\epsilon_r + 2\epsilon_m)^2 + \epsilon_i^2}] \tag{4.1}$$

When the denominator of the right hand side of equation 2.10 approaches zero, the extinction

cross-section approaches infinity. This condition is known as the resonance condition, but seems to be achievable only when $\epsilon_r$ approaches $-2\epsilon_m$ and when $\epsilon_i$ itself approaches zero.

It is the parameter $\epsilon_m$ that we can manipulate. It effectively acts as a transducer between a physical change in the local environment (the addition or removal of water from the polyelectrolyte) and a photonic signal (the absorption of particular wavelengths of light by LSPR). As this parameter shifts due to the uptake or loss of water, the wavelength corresponding to the SPR peak will shift. The degree of this shift should correspond to the change in the local dielectric constant from that of the polyelectrolyte multilayer to something closer to that of water. The requirement, then, is to create a polyelectrolyte film readily capable of swelling and deswelling upon changes in the local environment.

## 4.3 Methods

Polymer solutions of 0.01 M by repeat unit were developed by dissolving PAH ($M_w = 70,000$, Aldrich) and PAA (25% aqueous solution, $M_w = 90,000$, Polysciences) in 18 $M\Omega$ Ultrapure Water. These solutions were then acidified by the dropwise addition of HCl, reducing the pH of each solution to approximately 4.0.

The solutions could then be deposited onto the target substrates. For the spin-deposition process, the PAH was deposited first, followed by three rinse steps with 18 $M\Omega$ Ultrapure Water, then one layer of PAA, and another three rinse steps. The next layer of PAH was then deposited, and the process repeated until a film stack of the desired thickness was prepared. Each polymer spin-step was performed at 2,000 RPM for 30 seconds, while each rinse step was performed at 10,000 RPM, also at 30 seconds.

Completed films were then ready for silver infusion. The samples were allowed to rest in a 0.005

M silver acetate solution in ultrapure water solution for approximately one hour. The films were then dried and placed underneath a UV lamp for two hours to induce the formation of silver nanoparticles within the polyelectrolyte.

Two substrates were used with this film. The first, as with the silica NP-based sensor, consists of cut pieces of silicon wafer. Tests with this substrate were performed only with the base polyelectrolyte system without silver modification in order to investigate the swelling-deswelling and absorption-desorption behavior of the basic film, as well as to verify that deposition was indeed successful. The third substrate, the glass slide, was chosen to essentially eliminate the transparent polyelectrolyte film from the optical model, allowing us to monitor only absorption due to the presence of the silver nanoparticles.

Performed with both the silicon and glass slide substrates, all reflectometry measurements were taken within the same glove-box mentioned previously. As with those experiments the temperature was held constant at approximately $25^oC$. In these tests, the humidity within the box was adjusted by step changes of 10% RH from 10% RH to 90%. Each time the humidity set point was adjusted, the box was allowed to reach equilibrium and was left to stand for one minute before data was recorded. Once 90% RH was reached, the process was reversed, and measurements were taken again at every interval of 10% RH from 90% to 10%.

The model used for the silicon substrate was developed by fitting and adjusting the optical constants of the film stack until a suitable fit was achieved. This same material model was then used for all following tests with polyelectrolyte materials.

Rather than using the raw and unmolested transmission spectra as they are, common practice in the literature is to utilize Beer-Lambert's law to convert the percentage of light being transmitted

into a logarithmic scale like so:

$$A = 2 - log(T) \tag{4.2}$$

Where A is absorbance in absorption units (a.u.) and T is the percent of light transmitted through the media in question. The equation is designed such that at 100% transmission, A is zero.

## 4.4 Results and Discussion

### 4.4.1 Film Deposition and Nanoparticle Implantation

Spin coating a stack of polyelectrolyte onto silicon chips was successful, which is immediately obvious from the difference between the optical measurements of a baseline silicon wafer shard and that of the same chip with some layers of polylectrolyte deposited onto the surface, as seen by comparing the graphs in Figure 4.1 and 4.2.

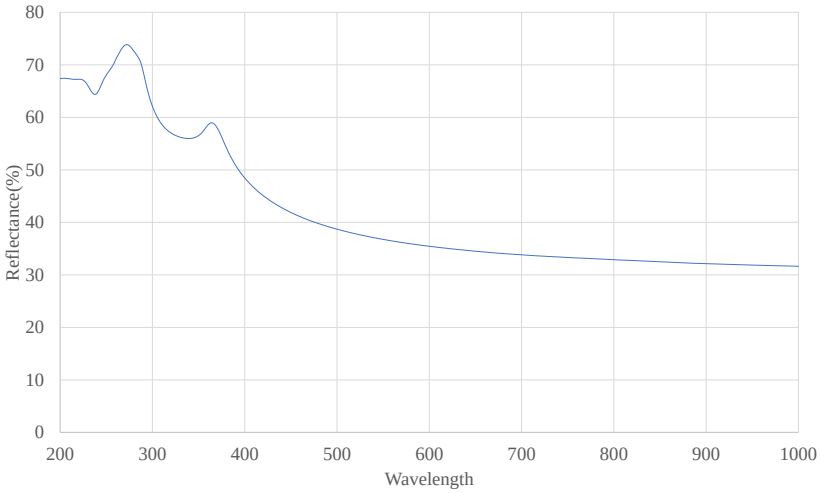


Figure 4.1: Reflectance of bare silicon wafer.

Deposition onto glass slides resulted in the formation of a transparent, colorless coating. Imme-

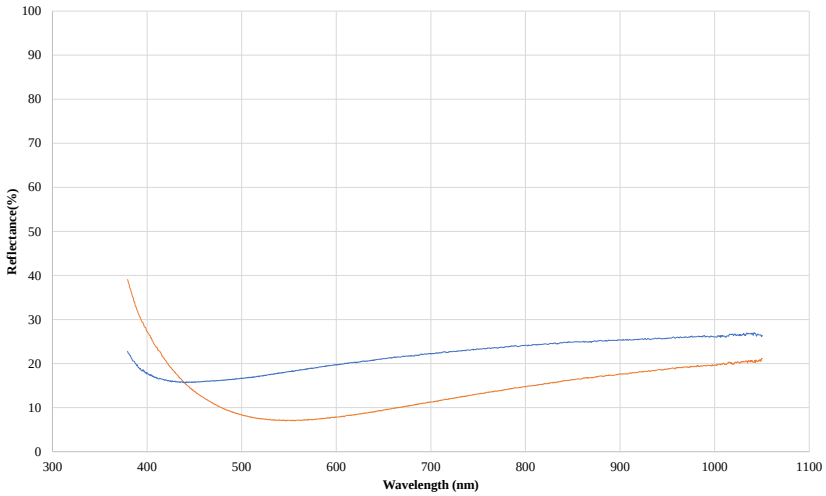


Figure 4.2: Reflectance of silicon wafer with polyelectrolyte bilayers with compositions of 10 PAA/10 PAH (Blue) and 15 PAA/15 PAH (Orange)

diately following impregnation, no significant visual change in the film was observed. This changed upon exposure to UV radiation, which caused the film to rapidly turn a vivid orange color. This contrast of pre and post exposure can be seen clearly in Figure 4.3.

The transmission spectra of the glass slide at different stages of preparation was required in order to evaluate whether the methodology did indeed result in the synthesis of silver nanoparticles which could exhibit a SPR response, or if the color change was due to some other unforeseen factors. The transmission spectra for a film prior to and following its impregnation with silver nitrate and exposure to two hours of UV radiation can be seen in Figure 4.4.

The presence of the sharp absorbance peak at 400 nanometers is strongly indicative of the SPR profile of silver nanoparticles. This seems to indicate that the silver nitrate and UV treatment was successful in generating the desired effect. We can then move on to examining the response of the films to humidity. However, it's important to evaluate the response of the base polyelectrolyte films before delving into the effect on the SPR wavelength.

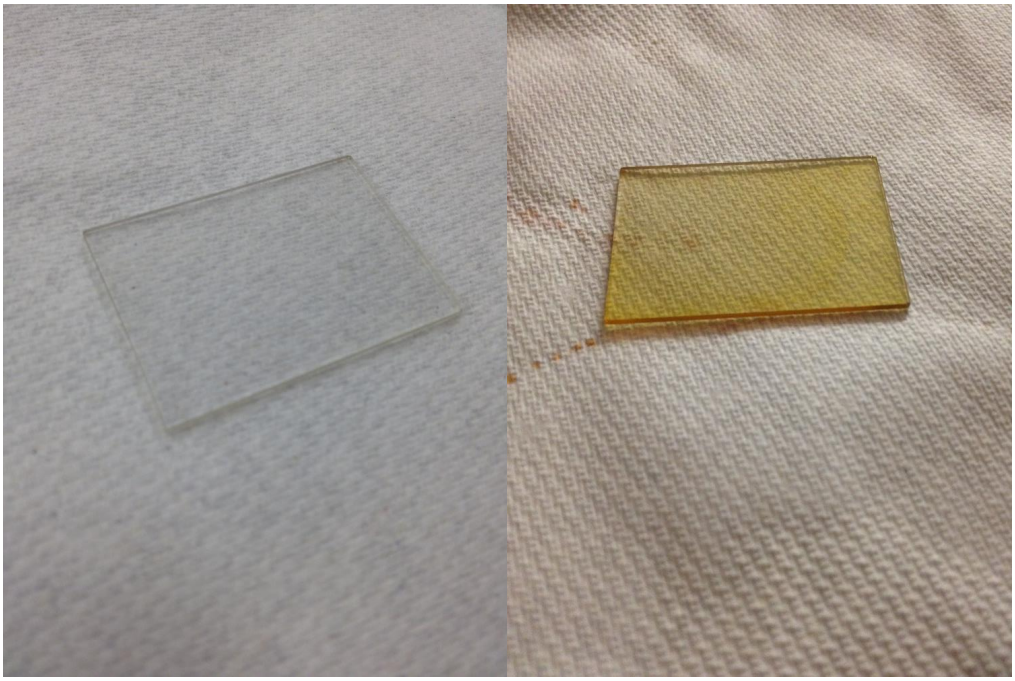

Figure 4.3: Photographs of 20-by-20 PAA-PAH PEM after impregnation with silver nitrate before (left) and after (right) exposure to UV light

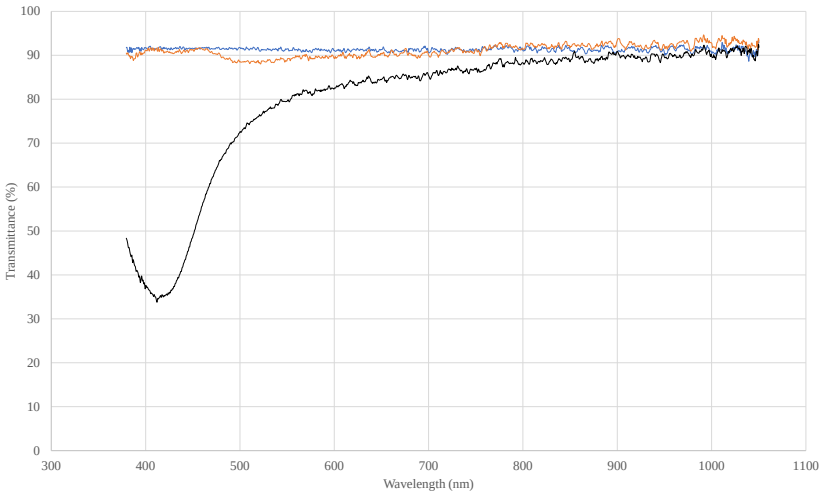


Figure 4.4: Transmission spectra of 20-by-20 PAA-PAH film on glass without modification (blue), after impregnation with silver nitrate (orange) and after exposure to UV light (black).

### 4.4.2 Humidity Response of Unmodified Polyelectrolyte Films

As previously mentioned, it's known that polyelectrolyte multilayer films will swell and deswell in response to changes in local humidity. The reflectance spectra in Figures 4.5 and 4.6 illustrate the effect that changing humidity has on the optical properties of these films. In all of these figures, the lines from brown to red correspond to 10%, 30%, 50%, 70%, 80% and 90% humidity, with the exception of the black line in 4.6 (b). Data for 70% humidity in this case was lost, and instead represents the optical response at 60% humidity.

In each case, the shift in optical response within the 400 to 1050 nm range began relatively gradually as humidity was increased from 10% to 20% and upwards. The change in optical properties seemed to accelerate as humidity increased, as can be seen by visually comparing the increasing gaps between each line. The same trend- with one exception that holds in all cases- can be seen in the case of decreasing humidity; the change in optical response only accelerated as the humidity approached the final set-point for the trial. Regardless of the direction of the change in humidity, however, shifting to or from 90% RH had the greatest effect on optical response.

This strange behavior around 90% RH must be taken with a grain of salt; fitting optical behavior at such high humidity proved difficult, even with the addition of a surface roughness layer and attempting to account for any possible misting on the surface of the film. Secrist and Nolte encountered similar difficulty with measuring the thickness of PAH and PAH/PAA films with humidity in excess of 90% RH. In the former case, they were even able to visually observe irregularities and non-uniformity in film thickness after exposure to these conditions.

In an attempt to understand the acceleration of change in optical parameters and the swelling-deswelling behavior associated with the films, both n and d have been graphed below in Figures 4.7

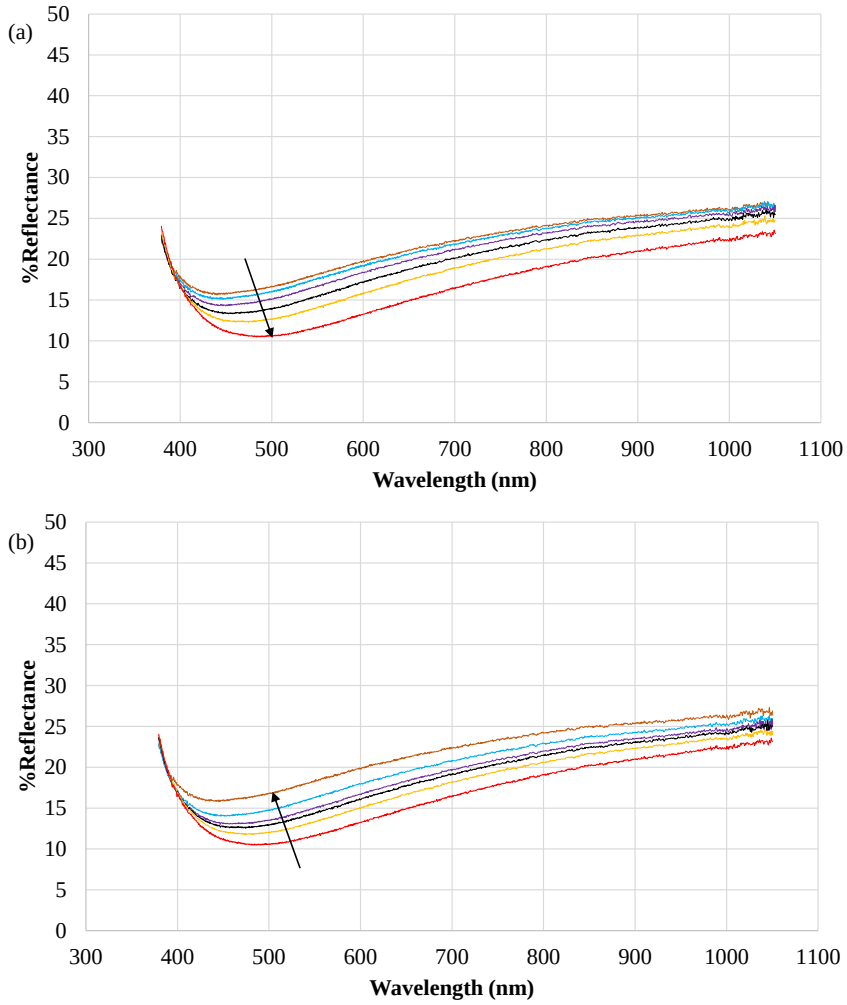


Figure 4.5: Reflectance spectra of 10-by-10 PAA-PAH film on bare silicon wafer under (a) rising and (b) falling humidity from 10% to 90% RH. Arrows denote the direction of the change in reflectance spectra.

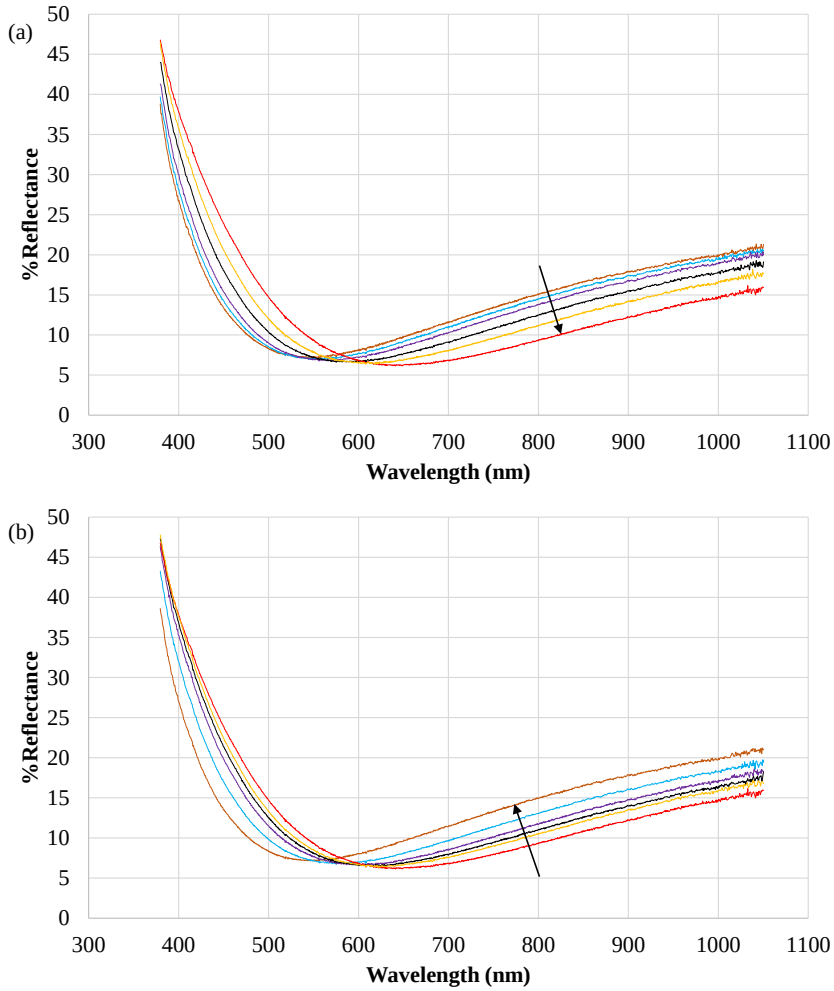


Figure 4.6: Reflectance spectra of 15-by-15 PAA-PAH film on bare silicon wafer under (a) rising and (b) falling humidity from 10% to 90% RH. Arrows denote the direction of the change in reflectance spectra.

and 4.8. It can be seen by the presence of an envelope in each of the graphs that the hysteresis we observe in the optical response has clear roots in the changing physical and optical properties of the films. This sorption hysteresis is similar to that which has been observed in certain biological systems, acid nafion membranes, montmolorillonite clays, crosslinked hydrocarbon resins and, indeed, in other experiments on PAH/PAA multilayers. [105, 106, 107, 108, 109, 110]

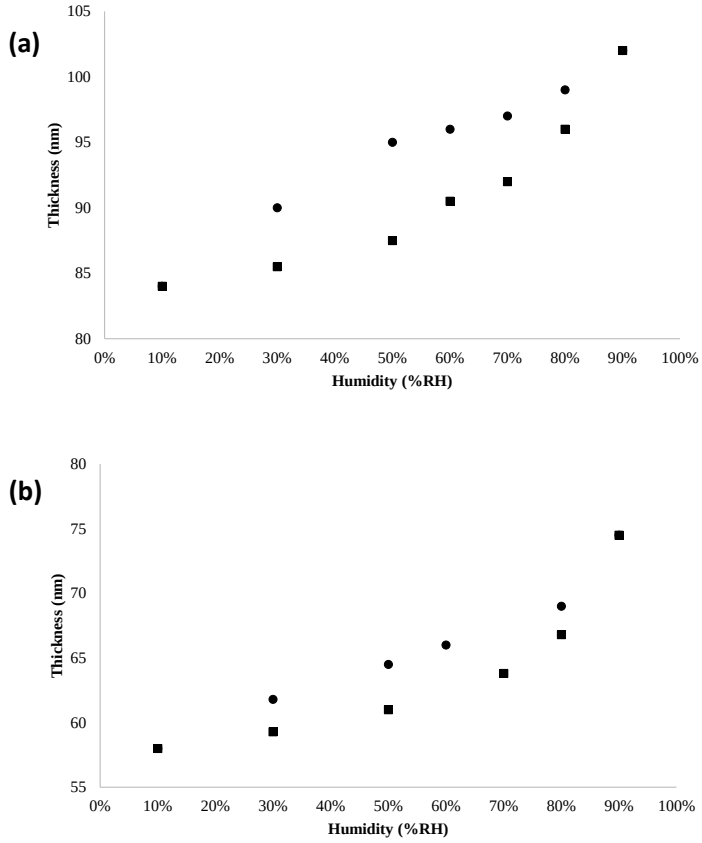


Figure 4.7: Thickness measurements of (a) 15-by-15 and (b) 10-by-10 PAA/PAH multilayer films under rising (squares) and falling (circles) humidity.

Secrist and Nolte suggested that the hysteresis is due to a rearrangement of the film structure. As water is taken up by the film, the film structures itself such that specific interactions between charged groups and water molecules becomes more favorable, and the rejection of water from the film becomes disfavored. This change in swelling behavior and the relatively rapid rise in thickness to the maximum at 90% RH compared to the more gradual fall in thickness as humidity is subsequently

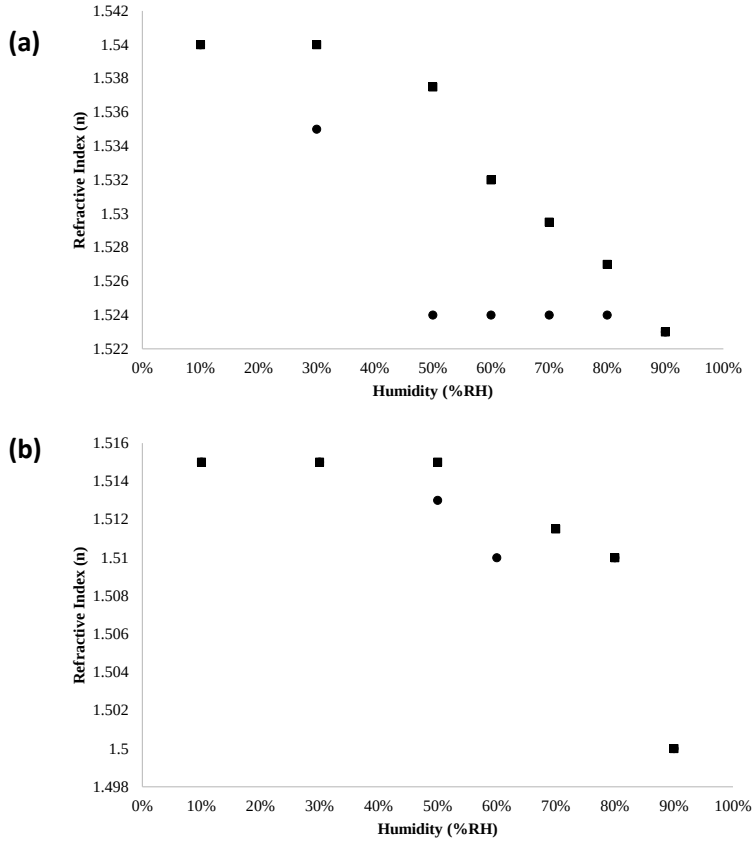


Figure 4.8: Refractive index measurements of (a) 15-by-15 and (b) 10-by-10 PAA/PAH multilayer films under rising (squares) and falling (circles) humidity.

decreased is due to this polymer rearrangement. Under normal conditions, the Flory-Huggins solution theory fits well with the behavior of films which transition in a relatively gradual and less pronounced way between swelling and deswelling moieties.

However, Secrist and Nolte were only able to properly fit their data when the solvent interaction parameter, $\chi$, was allowed to vary. Notably, they observed $\chi$ to decrease as humidity rose to negative values in PAH and near-zero in PAA films. This indicates that in both cases, the solvent interaction gradually became more favorable as more water was uptaken into the films. In the case of PAH, the solvent-polymer interaction became more favorable even than the intrachain interactions.

Although these expanded, swollen film structures were energetically favorable at high humidity, they cannot be maintained under conditions of lower humidity. While initially resisting the rejection of water from the films, the decreasing relative activity of water in the surrounding environment made solvent transport away from the films gradually more and more favorable. As water was removed, the forces preventing the films from recovering their original molecular structures diminished and the films collapsed. Subsequent rejection of solvent from the structure was unimpeded, hence the acceleration of the thinning process as humidity continued to decrease past the point at which the films had collapsed into their original conformation.

However, evidence contrary to the negative interaction parameter model comes from Tanchak et al.[111] Rather than observing a negative interaction parameter, they found in fact that PAA/PAH multilayers (pH unspecified) exhibit a very high interaction parameter with respect to water. Even ambient moisture at 100% humidity was found to be a poor solvent for the multilayer. Moreover, they found that the ionic charges of the PEM were largely screened by inter-entangled chains of opposite charge, which interacted preferentially with one another than with water entering the films. The exception to this is the top layer which, without the same degree of screening as the remainder of the

multilayer, is capable of interacting relatively more freely with ambient water.

This, however, doesn't quite adequately describe the reason for the hysteresis observed in the PEMs. Tanchak et al provide insights into the distribution of water in a PAA/PAH multilayer that might shed some light on the subject. It is known that the layers closer to the substrate are relatively more densely packed than those nearer to the surface. It's also known that the PAA in the lower layers have been shown to have a lower PKa, which reduces water solubility.[112] Tenchak et al found the water to be distributed asymmetrically in the vertical direction. A concentration gradient was observed to form across the thickness of the film stack, with the largest concentration found at the film/air interface and virtually no water at the substrate. Even after several hours- long enough for the film to reach some sort of equilibrium with the surrounding environment. They propose that the reason for this gradient is the occupation of microchannels through the film stack by water clusters in such a way that would prevent additional water vapor from percolating through the film. We can also hypothesize that the more densely packed layer closer to the substrate would more strongly resist water vapor percolation.

When the film reaches equilibrium with the surroundings, layer is in equilibrium with each adjacent layer, with the uppermost layers being relatively less densely packed and thus less resistant to infiltration by water. We can imagine, then, that as the first few layers saturate, some transport occurs by which water percolates down into lower layers. As humidity increases, more and more water percolates through the film, until the film layer density and the blocked pores prevent additional water from penetrating deeper. This may be what forces the first few layers apart and leads to the relatively loosely bound moisture noted by Secrist and Nolte to appear at 90% RH and above.

Some insight into what is transpiring in these films can be gleaned from the QCM data seen in Figure 4.9. For both curves, each step represents an increase or decrease of 10% RH between 10%

and 90% RH.

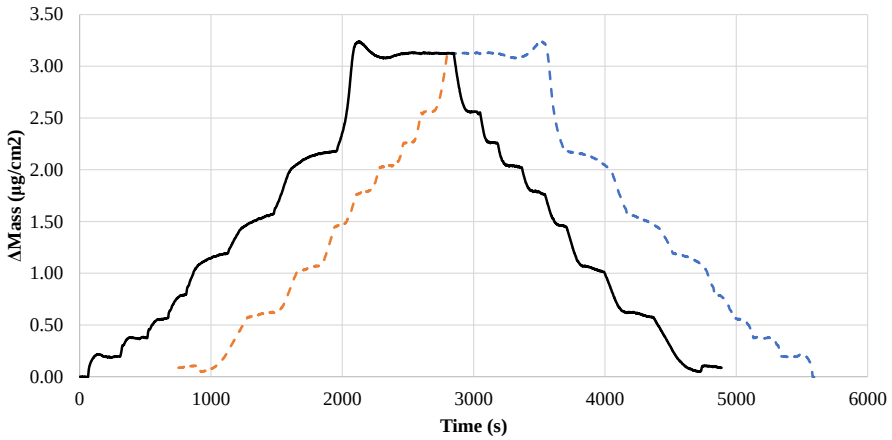


Figure 4.9: QCM data representing the absolute value of a change-in-mass for a 20-by-20 film under conditions of rising and falling humidity. Dotted orange and blue lines denote mirrored images of falling and rising data respectively to illustrate the nonlinearity associated with the response. For both curves, each step represents an increase or decrease of 10% RH between 10% and 90% RH.

The most interesting information to be gleaned from this graph is the strong nonlinearity associated with the film's mass changes in response to changing humidity. Starting from around 50% RH for either increasing or decreasing humidity, the film's mass begins to undergo more rapid changes compared to the earlier sections of either line. The notable exception is, once again, the shift from 90% RH to 80% RH, which is abnormally large by comparison to all other shifts.

This indicates that the change in the optical properties are unlikely to be due to a difference in the mass transport properties of the film itself. Contradicting Kugler's model, this film actually seems to take on more mass as humidity increases. Where Kugler et al. predicts that the addition of water to the film inhibits additional transport, the QCM results suggest that Secrist and Nolte's argument may be more accurate for these films. This would also explain why, even after several minutes, the films do not quite find a new steady state when ambient humidity is increased or decreased beyond the 50% RH point. That is, the films are undergoing some kind of structural change under relatively long time-scales that allow them to gradually absorb more and more water. The opposite effect occurs

under conditions of decreasing humidity; even after several minutes, mass continues to be lost and a steady-state is only apparently achieved at very long time scales.

The hysteresis, then, seems to come about as a result of these structural changes that affect how much water vapor the films are capable of solubilizing. It is of considerable interest to perform some kind of molecular simulation to evaluate exactly what sort of structural changes we might come to expect under these conditions, but such work is beyond the scope of this thesis. However due to the strong nonlinearity and hysteresis evidenced by the QCM data, it's clear that the PEM multilayers may not be the ideal choice for sensor design.

### 4.4.3 Effect of Humidity on SPR Peak Wavelength

In the end, the goal of this section of the project is not to spend time proselytizing on possible reasons behind the hysteresis behavior of these multilayer films. Rather, the goal is to determine whether, if at all, the relatively simplified preparation method outlined here can be used to develop useful optical sensors.

The trimmed results of one humidity sweep can be seen in Figure 4.10, with the area of most interest- the plasmon absorption peak- in focus in Figure 4.11. Each graph shows data taken at 10%, 50%, 70%, 80% and 90% RH from bottom to top. It was necessary to prune the data at 20%, 30%, 40% and 60% for readability's sake, as it would have otherwise shown considerable overlap among the lower curves, as seen in Figure 4.12.

Contrary to what had been hoped, there was a relatively insignificant amount of peak shifting associated with changes in humidity. The LSPR peak shifted by just over 2 nm under conditions of increasing humidity, and by approximately 3 nm under conditions of decreasing humidity, as seen

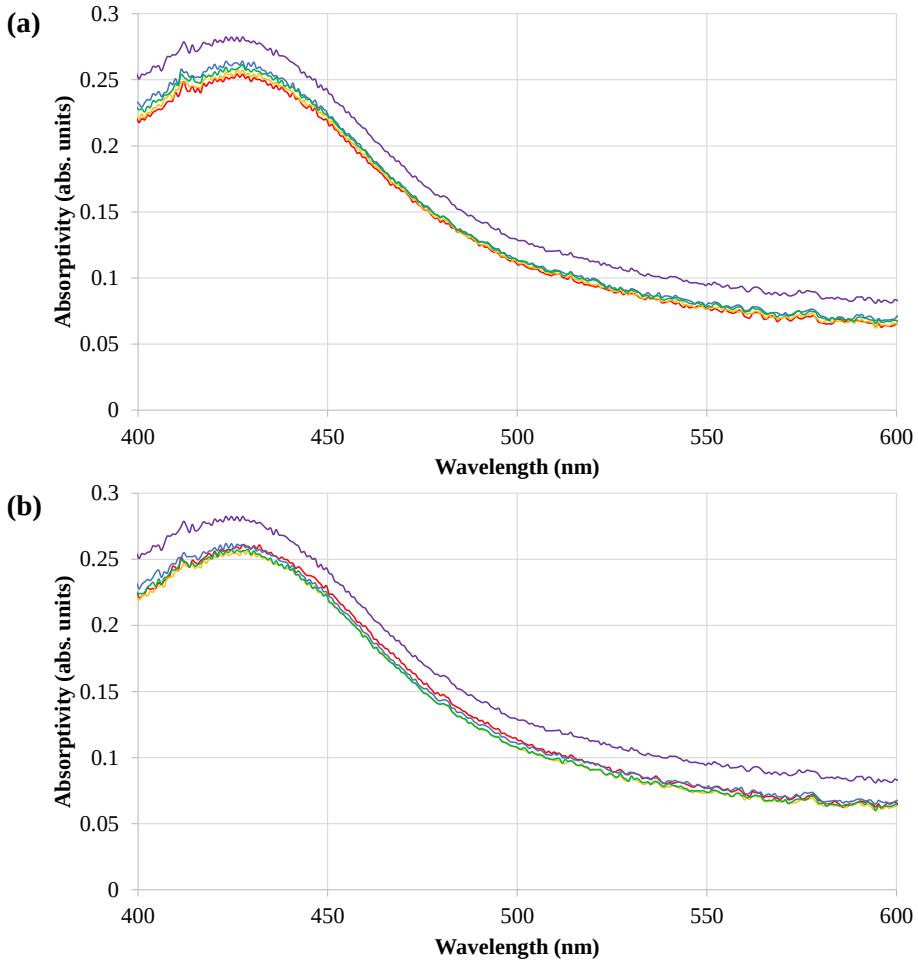


Figure 4.10: Absorption spectra of a 15-by-15 film with grown-in silver nanoparticles under (a) rising and (b) falling humidity conditions.

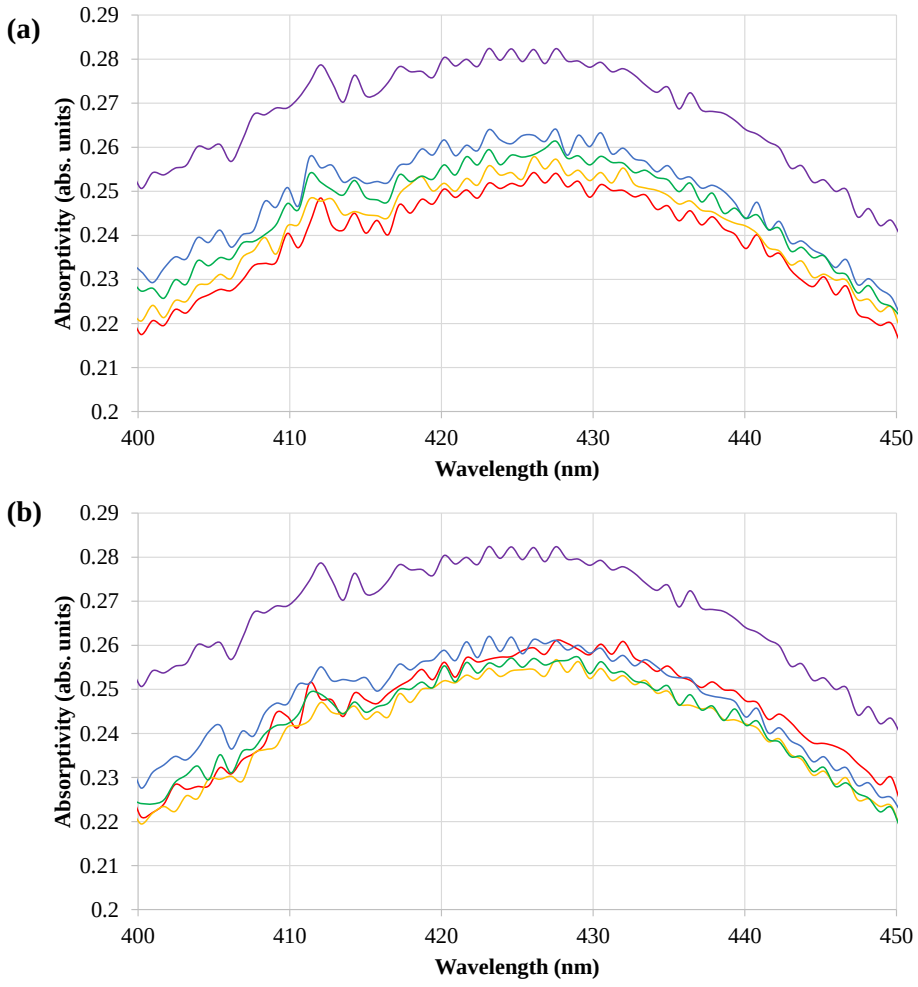


Figure 4.11: Absorption spectra with focus on the LSPR band of a 15-by-15 film with grown-in silver nanoparticles under (a) rising and (b) falling humidity conditions.

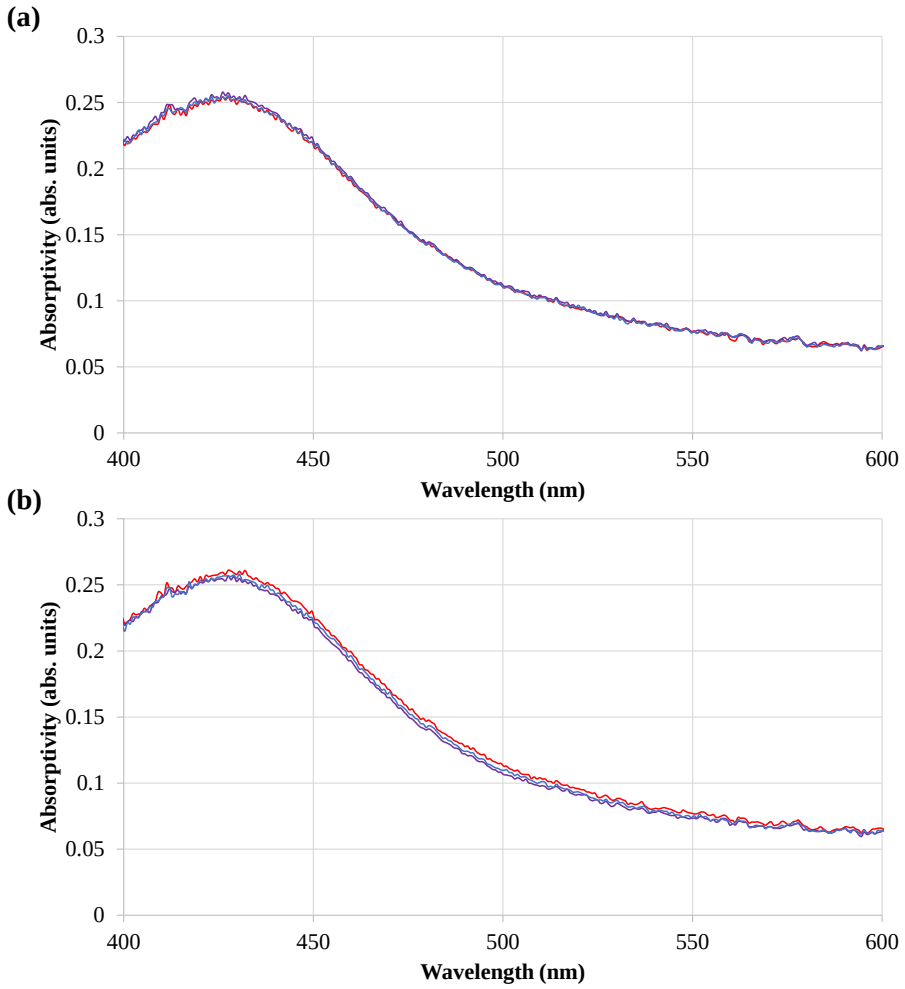


Figure 4.12: Absorption spectra at 10%, 30% and 50% humidity of a 15-by-15 film with grown-in silver nanoparticles under (a) rising and (b) falling humidity conditions.

in Figure 4.13. The peak location was estimated by fitting a quadratic function to the absorption data between 420 to 450 nm. The derivative of the resulting function was used to find the function's maximum point. We called this the peak location.

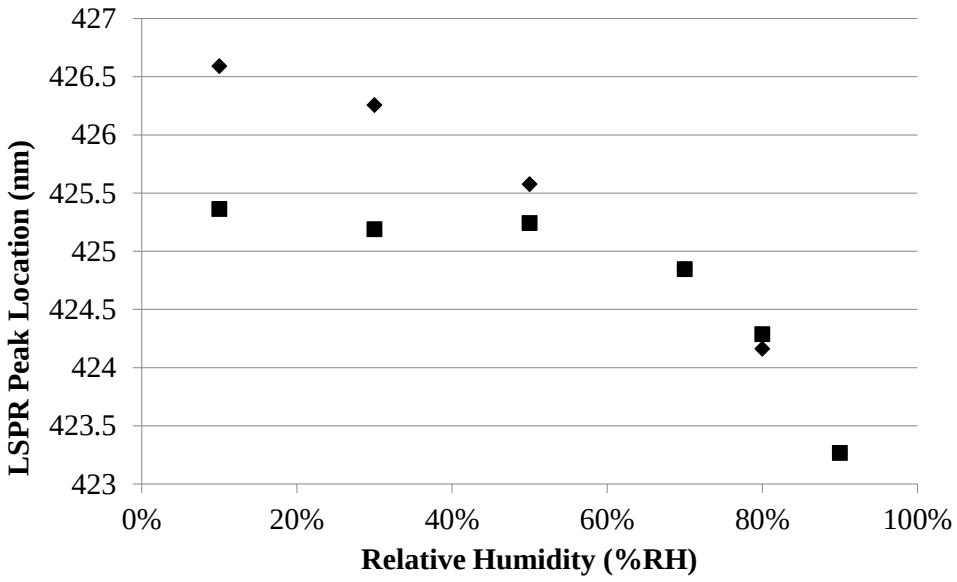


Figure 4.13: LSPR peak wavelength location of a 15-by-15 film under rising (diamonds) and falling (squares) humidity.

The cause of this is uncertain. One theory may be that, since the formation of silver nanoparticles is reliant on the nucleation of free ionic silver around free carboxylate groups, the silver NPs that do form essentially 'block' the absorption of water onto those same areas. In other words, while water vapor is clearly still entering the films and affecting the optical parameters (as can be clearly seen by the rise and fall of the absorptivity of the films), there is also little evidence that the water vapor is interacting in a meaningful way with the silver nanoparticles.

There does seem to be some specific and sensible change in the LSPR peak. Although so mild as to be almost indistinguishable from the optical response of the bulk film to changing humidity, it does appear that the peak absorbance increased slightly more in and around the LSPR peak compared to the rest of the film. However, it is extremely difficult to distinguish that this effect is present; the

difference in the response compared to an unmodified film is so slight that, aside from the utility of being able to specify a single wavelength to monitor, there seems to be little advantage over simply using the unmodified film in a reflective mode. Depending on the initial material state, we can use equation 4.1 to predict where the LSPR peak should shift. To illustrate the most extreme case, we begin with an initial state wherein the silver NPs are surrounded either by pure air or by pure PEM film, which corresponds to a peak location of 426.5 nm. The silver NPs are then submerged completely in water. If initially surrounded by air, the peak should shift to 649.1 nm. If originally in PEM, the peak would shift to 380.9 nm.[113, 114, 115]

No matter the case, the experimental results do not exhibit anywhere near as significant of a shift. If there is a specific, optically responsive effect specific to the interaction between absorbed atmospheric water vapor and the silver NPs, it seems to be relatively mild.

The hysteresis of the unmodified films is also still evident as is observed by the slightly increased spacing between the curves under 90% humidity in the rising humidity experiment compared to the nearly indistinguishable curves taken at the same, but falling, humidity. Notably, the jump from 80% to 90% humidity does seem to have a very significant and appreciable effect on the optical response. This may again be associated with the absorption of loosely-bound water into the film stack.

The key to the lack of responsiveness may be how the silver NPs were introduced into the system. In our films, silver NPs were grown directly into the stack after deposition was complete. A comparable study by Rivero et al. in 2012 showed a significantly more responsive film coating for an optical fiber-based sensor.[116] In their system, Rivero et al. had synthesized silver NPs through the use of silver nitrate with borane dimethylamine complex (DMAB) as a reducing agent. The NPs were capped by PAA. The anionic PAA electrolyte was then loaded with these synthesized NPs prior to stack assembly. They also used a dip-coating method rather than the spin-coating method described

here. Their results exhibited similar peak location to the ones reported here, though over a change of 20% to 70% humidity, they showed a change in absorbance in excess of 0.1 a.u., significantly more than what was observed in our experiments.

It's difficult to say exactly what structural difference might have resulted from the use of one method over another. We would need to use TEM or similar imaging techniques to examine cross-sections of the film structures to compare to one another to say for certain. That test is beyond the scope of this thesis.

## 4.5 Conclusions

We have shown here additional evidence supporting a structural change in the PAA/PAH PEM under exposure to high levels of humidity. It seems difficult to imagine that blockages local to the film's pores would alone result in the optical and QCM behavior shown here. However, in spite of those interesting results, it is difficult to qualify the development of these films into working sensors as a success. While there has been evidence of successes elsewhere using other means of introducing nanoparticles into the film stack, the combination of methods used here did not appear to create nanoparticle inclusions that meaningfully responded to changes in humidity.

# 5 CONCLUSIONS AND FUTURE WORK

## 5.1 Thesis Summary

The body of work making up this thesis represents several years of research into the optical properties and wetting-dewetting behavior of two very different film stacks under exposure to varying levels of humidity. In some ways, the work met with definite success.

The first chapter introduced the concept of thin-film sensors and summarized the contents of this thesis. The second chapter comprised a review over existing and historical humidity sensor technology, including a brief look into extant optical and electrical methods of monitoring humidity.

The third chapter launched properly into the background and details of the silicon NP sensor and the experiments performed to evaluate its performance. We demonstrated via ellipsometric methods that the aged, aggregated, silica NP film deposited using a single-step spin-coating method could serve as a highly responsive optical humidity sensor. QCM analysis demonstrated that the sensor was sensitive enough to detect and capture even the slight oscillations associated with the testing environment. We further demonstrated that water uptake in response to changing humidity conditions was indeed responsible for the shift in the film's refractive index by making use of a monochlorinated silane coating.

The fourth chapter examined the behavior of a PMA/PAH PEM film and detailed background information and a literature review of similar sensors. It was demonstrated that silver nanoparticles could be grown within the film stack by saturation with silver acetate and a subsequent UV-based

reduction step. Unfortunately, we also showed that the sensor was less responsive than desired. It did show interesting behavior at very high (> 80%) humidity, but the expected shifts in the peak SPR absorpton wavelength were so minor as to be undetectable, if they even existed at all. Despite this, the lack of responsiveness is in and of itself interesting, as literature showed that similar sensors developed using different techniques were in fact responsive. It might be interesting to investigate, going further, the differences between these two sensors and how they respond to changes in ambient humidity.

## 5.2 Future Work

### 5.2.1 Silane Modifications

The use of silanes in order to modify the chemistry of silica surfaces is well studied in the literature. Much of the work in chapter three demonstrated how effective silanes could be in massively reducing the hydrophilicity of the silica NP films. However, there are other, interesting applications for these molecules. Modification of mesoporous silica films for sensing organic molecules is well studied. For example, silica spheres with thiol surface groups were functionalized with 5,6-epoxyhexyltriethoxysilane, which enabled the detection of dopamine and glucosamine.[117] Another group modified a silica surface to detect the presence of specific pathogens by attaching an antibody to the silane's organic tail.[118]

Even more simple modifications, such as those performed by McAlpine et al. could be interesting to investigate.[119] In their work, McAlpine et al. used a nanowire sensor modified with alkane-, aldehyde- and amino-silanes to produce a so-called 'nano-electric nose' which could detect similar chemical vapors. In all of these systems, the silica was modified in such a way such that the silane

tail groups presented an attractive environment unto which particular chemicals could readily adhere. This produced a sensible change, either in the fluoresence of the films, or by inducing a chemical reaction, or by changing the electrical properties of the device.

We can imagine, then, a similar system for the optical sensing of hazardous chemical vapors. A silica NP film could be modified with a phenyl-silane to detect the presence of chemicals containing a benzene ring, for example. As benzene molecules move through the film pores, they would attach to the phenyls on the silane tails. As these accumulate, a fiber optic cable attached to a reflectometer could detect changes in the optical properties of the film. These molecules are flexible enough that any number of different chemicals might be tested for, which could have applications in a number of different areas, particularly in chemical lab and plant safety.

### 5.2.2 PEM Imaging

Of particular interest is determining the cause for the failure of the PEM-based sensor. One reason for why the silver NPs appeared to fail to respond to the addition of water to the PEM may be that they were somehow occluding or preventing the infiltration of water into their surrounding environment, possibly by occupying or otherwise monopolizing the charged groups in the PEM. In order to determine whether this is the case, it would be useful to use some kind of imaging technique to examine the distribution of water in the PEM network before and after NP modification and at various RH% points.

Tanchak et al. used neutron reflectometry to analyze the distribution of water in unmodified and salt-assembled PAA/PAH films.[112] While this would only potentially identify the interactions and location of water in relation to the nanoparticles, this data alone may be sufficient to determine what is happening in the films at the nano-scale. It would be interesting to compare and contrast the

behavior of the pre-mixed silver NP films with those we analyzed here. This may give some insight into why one method was successful whereas the other provided only lacklustre results.

Other analysis methods that could be interesting regardless of their applicability to solving this particular failure of function includes atomic force microscopy and scanning or transmission electron microscopy (AFM and SEM or TEM, respectively).[120] Both would give some indication as to the film structure and surface topography. However, traditional electron microscopy requires operation in vacuum, rendering any humidity-effects null.

An interesting way to capture the conformation of the films under different levels of humidity (particularly at the high range, when we actually did observe some promising behavior) is through Cryo-TEM. As the name suggests, Cryo-TEM involves first rapidly reducing the temperature of the sample, thus freezing most if not all of the water into vitrified ice.[121] This structure can then be analyzed via TEM. While most Cryo-TEM has been performed on aqueous solutions or liquid-phase suspensions, it does not seem impossible to develop a methodology for the application of Cryo-TEM to these hydrophilic films, and could provide critical insight into the change in film morphology as humidity rises and falls.[122, 123]

### 5.2.3 Mechanical and Biofouling Tests

In order to further evaluate the robustness of the films, two major factors should be accounted for. The first is the mechanical properties of the films, specifically their resistance to abrasion, damage and deformation. The optical models used to interrogate the film stacks rely on relatively uniform layers; it stands to reason that any damage to the surface of the films would necessarily be troublesome indeed. However, it is also worthwhile to determine the flexile and tensile properties of the films as well; while glass is an appropriate substrate for laboratory-scale experiments, it may be more cost-effective

to utilize a thinner, more pliable material that can easily be used in roll-to-roll manufacturing. For such an application, it would be necessary to evaluate to what degree the films can endure long-term deformation without loss of functionality.

However, more interesting is the possibility of biofouling, specifically by the growth of bacteria or other microorganisms through the film stack. Humid conditions are ideal for the growth of many microorganisms, and any sensor which is exposed to these environs for prolonged periods would almost certainly be susceptible to infiltration by undesirable growths. While the silver NPs in the PEM are well known for their antimicrobial properties, the silica film is unprotected. It would be of use to determine whether microbial infiltration is a serious risk to the long-term operation of these films, and whether there are available methods to render the films more resistant to infection.[124]

# LIST OF REFERENCES

[1] David M. Gann. Building Innovation: Complex Constructs in a Changing World. Thomas Telford Publishing, jan 2000.

[2] Joseph R. Stetter, William R. Penrose, and Sheng Yao. Sensors, chemical sensors, electrochemical sensors, and ECS. Journal of The Electrochemical Society, 150(2):S11, 2003.

[3] Arun S. Mujumdar. MOISTURE SENSORS IN PROCESS CONTROL. Drying Technology, 5(3):485–486, aug 1987.

[4] E.J. Connolly, G.M. O'Halloran, H.T.M. Pham, P.M. Sarro, and P.J. French. Comparison of porous silicon, porous polysilicon and porous silicon carbide as materials for humidity sensing applications. Sensors and Actuators A: Physical, 99(1-2):25–30, apr 2002.

[5] Lei Xu, Rui Wang, Qi Xiao, Dan Zhang, and Yong Liu. Micro humidity sensor with high sensitivity and quick response/recovery based on ZnO/TiO2composite nanofibers. Chinese Physics Letters, 28(7):070702, jul 2011.

[6] A W Brewer, B Cwilong, and G M B Dobson. Measurement of absolute humidity in extremely dry air. Proceedings of the Physical Society, 60(1):52–70, jan 1948.

[7] Stanley H. Jury, Louis P. Bosanquet, and Young W. Kim. Fast response sensing element for a frost point hygrometer. Review of Scientific Instruments, 38(11):1634–1637, nov 1967.

[8] KTV Grattan, ZY Zhang, T Sun, Yonghang Shen, Limin Tong, and Zhuchang Ding. Sapphire-

ruby single-crystal fibre for application in high temperature optical fibre thermometers: studies at temperatures up to 1500 c. Measurement Science and Technology, 12(7):981, 2001.

[9] J. Lin, M. Heurich, and E. Obermeier. Manufacture and examination of various spin-on glass films with respect to their humidity-sensitive properties. Sensors and Actuators B: Chemical, 13(1-3):104–106, may 1993.

[10] M. D'Apuzzo, A. Aronne, S. Esposito, and P. Pernice. Sol-gel synthesis of humidity-sensitive p2o5-sio2 amorphous films. Journal of Sol-Gel Science and Technology, 17(3):247–254, 2000.

[11] L. B. Kong, L. Y. Zhang, and X. Yao. Preparation and properties of a humidity sensor based on licl-doped porous silica. Journal of Materials Science Letters, 16(10):824–826, 1997.

[12] Chien-Tsung Wang, Chun-Lung Wu, I-Cherng Chen, and Yi-Hsiao Huang. Humidity sensors based on silica nanoparticle aerogel thin films. Sensors and Actuators B: Chemical, 107(1):402–410, may 2005.

[13] Hamid Farahani, Rahman Wagiran, and Mohd Hamidon. Humidity sensors principle, mechanism, and fabrication technologies: A comprehensive review. Sensors, 14(5):7881–7939, apr 2014.

[14] Bernard M. Kulwicki. Humidity sensors. Journal of the American Ceramic Society, 74(4):697–708, apr 1991.

[15] Zhi Chen and Chi Lu. Humidity sensors: A review of materials and mechanisms. Sensor Letters, 3(4):274–295, dec 2005.

[16] T. Seiyama, N. Yamazoe, and H. Arai. Ceramic humidity sensors. Sensors and Actuators,

4:85–96, jan 1983.

[17] Kimberly E. Secrist and Adam J. Nolte. Humidity swelling/deswelling hysteresis in a polyelectrolyte multilayer film. Macromolecules, 44(8):2859–2865, apr 2011.

[18] Kevin T. Cook, Kwadwo E. Tettey, Robert M. Bunch, Daeyeon Lee, and Adam J. Nolte. One-step index-tunable antireflection coatings from aggregated silica nanoparticles. ACS Applied Materials & Interfaces, 4(12):6426–6431, dec 2012.

[19] B. E. Conway, J. O. M. Bockris, and Hedda Linton. Proton conductance and the existence of the h3o ion. The Journal of Chemical Physics, 24(4):834–850, apr 1956.

[20] Colin A. Wraight. Chance and design—proton transfer in water, channels and bioenergetic proteins. Biochimica et Biophysica Acta (BBA) - Bioenergetics, 1757(8):886–912, aug 2006.

[21] Jie Liu, Mangilal Agarwal, Kody Varahramyan, Ernest S. Berney, and Wayne D. Hodo. Polymer-based microsensor for soil moisture measurement. Sensors and Actuators B: Chemical, 129(2):599–604, feb 2008.

[22] S. Tsuchitani, T. Sugawara, N. Kinjo, S. Ohara, and T. Tsunoda. A humidity sensor using ionic copolymer and its application to a humidity-temperature sensor module. Sensors and Actuators, 15(4):375–386, dec 1988.

[23] Karen L. Rauen, Doris A. Smith, William R. Heineman, Jay Johnson, Russell Seguin, and Paul Stoughton. Humidity sensor based on conductivity measurements of a poly(dimethyldiallylammonium chloride) polymer film. Sensors and Actuators B: Chemical, 17(1):61–68, nov 1993.

[24] Noam Agmon. The grotthuss mechanism. Chemical Physics Letters, 244(5-6):456–462, oct

1995.

[25] Noboru Yamazoe and Yasuhiro Shimizu. Humidity sensors: Principles and applications. Sensors and Actuators, 10(3-4):379–398, nov 1986.

[26] P.M. Harrey, B.J. Ramsey, P.S.A. Evans, and D.J. Harrison. Capacitive-type humidity sensors fabricated using the offset lithographic printing process. Sensors and Actuators B: Chemical, 87(2):226–232, dec 2002.

[27] Qiaohui Zhang, J.R. Smith, L.V. Saraf, and Feng Hua. Transparent humidity sensor using cross-linked polyelectrolyte membrane. IEEE Sensors Journal, 9(7):854–857, jul 2009.

[28] M. Matsuguchi, M. Shinmoto, Y. Sadaoka, T. Kuroiwa, and Y. Sakai. Effect of the degree of cross-linking on the characteristics of a PVCA capacitive-type humidity sensor. Sensors and Actuators B: Chemical, 34(1-3):349–355, aug 1996.

[29] MP De Jong, LJ Van Ijzendoorn, and MJA De Voigt. Stability of the interface between indium-tin-oxide and poly (3, 4-ethylenedioxythiophene)/poly (styrenesulfonate) in polymer light-emitting diodes. Applied Physics Letters, 77(14):2255–2257, 2000.

[30] Kuan Sun, Shupeng Zhang, Pengcheng Li, Yijie Xia, Xiang Zhang, Donghe Du, Furkan Halis Isikgor, and Jianyong Ouyang. Review on application of pedots and pedot: Pss in energy conversion and storage devices. Journal of Materials Science: Materials in Electronics, 26(7):4438–4462, 2015.

[31] A.R.K. Ralston, C.F. Klein, P.E. Thomas, and D.D. Denton. A model for the relative environmental stability of a series of polyimide capacitance humidity sensors. In Proceedings of the International Solid-State Sensors and Actuators Conference. IEEE.

[32] M. Dokmeci and K. Najafi. A high-sensitivity polyimide capacitive relative humidity sensor for monitoring anodically bonded hermetic micropackages. Journal of Microelectromechanical Systems, 10(2):197–204, jun 2001.

[33] S.N. Chen, E.S. Ramakrishnan, R.S. Huang, and W.W. Grannemann. A new thin-film humidity microsensor. IEEE Electron Device Letters, 5(11):452–453, nov 1984.

[34] J T W Yeow and J P M She. Carbon nanotube-enhanced capillary condensation for a capacitive humidity sensor. Nanotechnology, 17(21):5441–5448, oct 2006.

[35] Cecilia Roman, Olimpiu Bodea, Nicolae Prodan, Andrei Levi, Emil Cordos, and Ionel Manoviciu. A capacitive-type humidity sensor using crosslinked poly(methyl methacrylate-co-(2 hydroxypropyl)-methacrylate). Sensors and Actuators B: Chemical, 25(1-3):710–713, apr 1995.

[36] Narsimha Parvatikar, Shilpa Jain, Syed Khasim, M. Revansiddappa, S.V. Bhoraskar, and M.V.N. Ambika Prasad. Electrical and humidity sensing properties of polyaniline/WO3 composites. Sensors and Actuators B: Chemical, 114(2):599–603, apr 2006.

[37] R.P. Tandon, M.R. Tripathy, A.K. Arora, and Surat Hotchandani. Gas and humidity response of iron oxide—polypyrrole nanocomposites. Sensors and Actuators B: Chemical, 114(2):768–773, apr 2006.

[38] Pi-Guey Su and Chia-Pin Wang. Flexible humidity sensor based on TiO2 nanoparticles-polypyrrole-poly-[3-(methacrylamino)propyl] trimethyl ammonium chloride composite materials. Sensors and Actuators B: Chemical, 129(2):538–543, feb 2008.

[39] Dewyani Patil and Pradip Patil. A rapid response humidity sensor based on poly(2, 5-dimethoxyaniline)-tin oxide nanocomposite. Sensor Letters, 9(4):1298–1308, aug 2011.

[40] Aoife C. Power, Anthony J. Betts, and John F. Cassidy. Silver nanoparticle polymer composite based humidity sensor. The Analyst, 135(7):1645, 2010.

[41] Norman A. Luechinger, Stefan Loher, Evagelos K. Athanassiou, Robert N. Grass, and Wendelin J. Stark. Highly sensitive optical detection of humidity on polymer/metal nanoparticle hybrid films. Langmuir, 23(6):3473–3477, mar 2007.

[42] Tetsuo Morimoto, Mahiko Nagao, and Fujiko Tokuda. Relation between the amounts of chemisorbed and physisorbed water on metal oxides. The Journal of Physical Chemistry, 73(1):243–248, jan 1969.

[43] O S Heavens. Optical properties of thin films. Reports on Progress in Physics, 23(1):1–65, jan 1960.

[44] Cauchy's dispersion formula. In Encyclopedic Dictionary of Polymers, pages 167–167. Springer New York.

[45] Ivan D. Nikolov and Christo D. Ivanov. Optical plastic refractive measurements in the visible and the near-infrared regions. Applied Optics, 39(13):2067, may 2000.

[46] Jan W. Gooch. Sellmeier equation. In Encyclopedic Dictionary of Polymers, pages 653–654. Springer New York, 2011.

[47] Neal J Hutchinson, Thomas Coquil, Ashcon Navid, and Laurent Pilon. Effective optical properties of highly ordered mesoporous thin films. Thin Solid Films, 518(8):2141–2146, 2010.

[48] Bulent E Yoldas. Investigations of porous oxides as an antireflective coating for glass surfaces. Applied Optics, 19(9):1425–1429, 1980.

[49] A.H. Sihvola and Institution of Electrical Engineers. Electromagnetic Mixing Formulas and Applications. Electromagnetics and Radar Series. Institution of Electrical Engineers, 1999.

[50] CM Herzinger, B Johs, WA McGahan, John A Woollam, and W Paulson. Ellipsometric determination of optical constants for silicon and thermally grown silicon dioxide via a multi-sample, multi-wavelength, multi-angle investigation. Journal of Applied Physics, 83(6):3323–3336, 1998.

[51] Magdalena D. Anguelova. Complex dielectric constant of sea foam at microwave frequencies. Journal of Geophysical Research, 113(C8), aug 2008.

[52] Jacques Curie and Pierre Curie. Piezo-electric and allied phenomena in rochelle salt. Comptes Rendus de l'Acadmie des Sciences, 91:294–297, mar 1880.

[53] Günter Sauerbrey. Verwendung von schwingquarzen zur wägung dünner schichten und zur mikrowägung. Zeitschrift für Physik, 155(2):206–222, apr 1959.

[54] Lord Rayleigh. On the free vibrations of an infinite plate of homogeneous isotropic elastic matter. Proceedings of the London Mathematical Society, s1-20(1):225–237, nov 1888.

[55] Kenneth A. Marx. Quartz crystal microbalance: a useful tool for studying thin polymer films and complex biomolecular systems at the solution-surface interface. Biomacromolecules, 4(5):1099–1120, sep 2003.

[56] Christopher C. White and John L. Schrag. Theoretical predictions for the mechanical response of a model quartz crystal microbalance to two viscoelastic media: A thin sample layer and surrounding bath medium. The Journal of Chemical Physics, 111(24):11192–11206, dec 1999.

[57] Bryan D. Vogt, Eric K. Lin, Wen li Wu, and Christopher C. White. Effect of film thickness on the validity of the sauerbrey equation for hydrated polyelectrolyte films. The Journal of Physical Chemistry B, 108(34):12685–12690, aug 2004.

[58] Seung-Sub Lee, Jong-Dal Hong, Chang Hwan Kim, Kwan Kim, Ja Pil Koo, and Ki-Bong Lee. Layer-by-layer deposited multilayer assemblies of ionene-type polyelectrolytes based on the spin-coating method. Macromolecules, 34(16):5358–5360, jul 2001.

[59] Dinguo Chen. Anti-reflection (AR) coatings made by sol–gel processes: A review. Solar Energy Materials and Solar Cells, 68(3-4):313–336, jun 2001.

[60] Timothy J. Rehg and G. Higgins. Spin coating of colloidal suspensions. AIChE Journal, 38(4):489–501, apr 1992.

[61] D. E. Bornside, C. W. Macosko, and L. E. Scriven. Spin coating: One-dimensional model. Journal of Applied Physics, 66(11):5185–5193, dec 1989.

[62] C.J. Brinker, A.J. Hurd, P.R. Schunk, G.C. Frye, and C.S. Ashley. Review of sol-gel thin film formation. Journal of Non-Crystalline Solids, 147-148:424–436, jan 1992.

[63] Dietrich Meyerhofer. Characteristics of resist films produced by spinning. Journal of Applied Physics, 49(7):3993–3997, jul 1978.

[64] David S. Nyce. Position Sensors. John Wiley & Sons, Inc., jun 2016.

[65] R. K. ILER. Adsorption of colloidal silica on alumina and of colloidal alumina on silica. Journal of the American Ceramic Society, 47(4):194–198, apr 1964.

[66] R.K. Iler. Multilayers of colloidal particles. Journal of Colloid and Interface Science, 21(6):569–594, jun 1966.

[67] Daeyeon Lee, Michael F. Rubner, and Robert E. Cohen. All-nanoparticle thin-film coatings. Nano Letters, 6(10):2305–2312, oct 2006.

[68] Janos H. Fendler, editor. Nanoparticles and Nanostructured Films. Wiley-VCH Verlag GmbH, may 1998.

[69] Andrea Bearzotti, Johnny Mio Bertolo, Plinio Innocenzi, Paolo Falcaro, and Enrico Traversa. Humidity sensors based on mesoporous silica thin films synthesised by block copolymers. Journal of the European Ceramic Society, 24(6):1969–1972, jan 2004.

[70] Zi-Le Hua, Jian-Lin Shi, Lin Wang, and Wen-Hua Zhang. Preparation of mesoporous silica films on a glass slide: surfactant template removal by solvent extraction. Journal of Non-Crystalline Solids, 292(1-3):177–183, nov 2001.

[71] L. Y. Zhao, K. R. Eldridge, K. Sukhija, H. Jalili, N. F. Heinig, and K. T. Leung. Electrodeposition of iron core-shell nanoparticles on a h-terminated si(100) surface. Applied Physics Letters, 88(3):033111, jan 2006.

[72] Bernadette M. Quinn, Cees Dekker, and Serge G. Lemay. Electrodeposition of noble metal nanoparticles on carbon nanotubes. Journal of the American Chemical Society, 127(17):6146–6147, may 2005.

[73] S Kolliopoulou, D Tsoukalas, P Dimitrakis, P Normand, S Paul, C Pearson, A Molloy, and M C Petty. Field effect devices with metal nanoparticles integrated by langmuir–blodgett technique for non-volatile memory applications. Journal of Physics: Conference Series, 10:57–60, jan 2005.

[74] M. Brust, N. Stuhr-Hansen, K. Norgaard, J.B. Christensen, Lars Kildemark Nielsen, and T. Bjornholm. Langmuir-blodgett films of alkane chalcogenice (s, se, te) stabilized gold

nanoparticles. Nano Letters, 1(4):189–191, 2001.

[75] Yong-Jae Choi, Chi-Kai Chiu, and Tzy-Jiun M Luo. Spontaneous deposition of gold nanoparticle nanocomposite on polymer surfaces through sol-gel chemistry. Nanotechnology, 22(4):045601, dec 2010.

[76] Yot Boontongkong, Robert E. Cohen, and Michael F. Rubner. Selective electroless copper deposition within block copolymer microdomains. Chemistry of Materials, 12(6):1628–1633, jun 2000.

[77] David Levy and Marcos Zayat. The Sol-Gel Handbook: Synthesis, Characterization and Applications, 3-Volume Set. Wiley-VCH, 2015.

[78] Javier Bravo, Lei Zhai, Zhizhong Wu, Robert E. Cohen, and Michael F. Rubner. Transparent superhydrophobic films based on silica nanoparticles. Langmuir, 23(13):7293–7298, jun 2007.

[79] W. J. Eakins. Silanol groups on silica and their reactions with trimethyl chlorosilane and trimethysilanol. Industrial & Engineering Chemistry Product Research and Development, 7(1):39–43, mar 1968.

[80] J. D. Le Grange, J. L. Markham, and C. R. Kurkjian. Effects of surface hydration on the deposition of silane monolayers on silica. Langmuir, 9(7):1749–1753, jul 1993.

[81] Minghua Yu, Guotuan Gu, Wei-Dong Meng, and Feng-Ling Qing. Superhydrophobic cotton fabric coating based on a complex layer of silica nanoparticles and perfluorooctylated quaternary ammonium silane coupling agent. Applied Surface Science, 253(7):3669–3673, jan 2007.

[82] Eric Tyrode and Jonathan F. D. Liljeblad. Water structure next to ordered and disordered hy-

drophobic silane monolayers: A vibrational sum frequency spectroscopy study. The Journal of Physical Chemistry C, 117(4):1780–1790, jan 2013.

[83] Alexandra Ancelmo Piscitelli Mansur, Otavio Luiz do Nascimento, Wander Luiz Vasconcelos, and Herman Sander Mansur. Chemical functionalization of ceramic tile surfaces by silane coupling agents: polymer modified mortar adhesion mechanism implications. Materials Research, 11(3):293–302, sep 2008.

[84] Wei Li, Baoquan Zhou, Mingyu Wang, Zhonghui Li, and Rong Ren. Silane functionalization of graphene oxide and its use as a reinforcement in bismaleimide composites. Journal of Materials Science, 50(16):5402–5410, 08 2015.

[85] C. Rodriguez, P. Laplace, D. Gallach-Prez, P. Pellacani, R.J. Martn-Palma, V. Torres-Costa, G. Ceccone, and M. Manso Silvn. Hydrophobic perfluoro-silane functionalization of porous silicon photoluminescent films and particles. Applied Surface Science, 380(Supplement C):243 – 248, 2016. Proceedings for International Conference on Surfaces, Coatings and Nanostructured Materials (NANOSMAT-10, Manchester, UK).

[86] Alexander Y. Fadeev and Thomas J. McCarthy. Self-assembly is not the only reaction possible between alkyltrichlorosilanes and surfaces: monomolecular and oligomeric covalently attached layers of dichloro- and trichloroalkylsilanes on silicon. Langmuir, 16(18):7268–7274, sep 2000.

[87] Man Lung Sham, Jing Li, Peng Cheng Ma, and Jang-Kyo Kim. Cleaning and functionalization of polymer surfaces and nanoscale carbon fillers by UV/ozone treatment: A review. Journal of Composite Materials, 43(14):1537–1564, jun 2009.

[88] Lewis Greenspan et al. Humidity fixed points of binary saturated aqueous solutions. Journal of

research of the national bureau of standards, 81(1):89–96, 1977.

[89] R Collins. The choice of an effective time constant for diffusive processes in finite systems (thermal conduction and sputtering examples). Journal of Physics D: Applied Physics, 13(11):1935–1947, nov 1980.

[90] Edward L. Pinnes. Time constants for moisture diffusion through a permeable barrier into an airspace. Polymer Engineering and Science, 19(7):525–529, may 1979.

[91] H. Park. Characterization of moisture diffusion into polymeric thin film. Experimental Mechanics, 53(9):1693–1703, jul 2013.

[92] Sylvia Underwood and Paul Mulvaney. Effect of the solution refractive index on the color of gold colloids. Langmuir, 10(10):3427–3430, oct 1994.

[93] Zhi mei Qi, Itaru Honma, and Haoshen Zhou. Humidity sensor based on localized surface plasmon resonance of multilayer thin films of gold nanoparticles linked with myoglobin. Optics Letters, 31(12):1854, jun 2006.

[94] Z.M. Rittersma. Recent achievements in miniaturised humidity sensors—a review of transduction techniques. Sensors and Actuators A: Physical, 96(2-3):196–210, feb 2002.

[95] Jiri Homola, Sinclair S. Yee, and Gunter Gauglitz. Surface plasmon resonance sensors: review. Sensors and Actuators B: Chemical, 54(1-2):3–15, jan 1999.

[96] B. Chadwick and M. Gal. Enhanced optical detection of hydrogen using the excitation of surface plasmons in palladium. Applied Surface Science, 68(1):135–138, may 1993.

[97] Petr Tobiska, Olivier Hugon, Alain Trouillet, and Henri Gagnaire. An integrated optic hydrogen sensor based on SPR on palladium. Sensors and Actuators B: Chemical, 74(1-3):168–172,

apr 2001.

[98] Jiri Homola, Hana Vaisocherova, Jakub Dostalek, and Marek Piliarik. Multi-analyte surface plasmon resonance biosensing. Methods, 37(1):26–36, sep 2005.

[99] Jiri Homola. Surface plasmon resonance sensors for detection of chemical and biological species. Chemical Reviews, 108(2):462–493, feb 2008.

[100] G. Decher, J.D. Hong, and J. Schmitt. Buildup of ultrathin multilayer films by a self-assembly process: III. consecutively alternating adsorption of anionic and cationic polyelectrolytes on charged surfaces. Thin Solid Films, 210-211:831–835, apr 1992.

[101] Tom C. Wang, Michael F. Rubner, and Robert E. Cohen. Polyelectrolyte multilayer nanoreactors for preparing silver nanoparticle composites: controlling metal concentration and nanoparticle size. Langmuir, 18(8):3370–3375, apr 2002.

[102] P.A. Chiarelli, M.S. Johal, J.L. Casson, J.B. Roberts, J.M. Robinson, and H.-L. Wang. Controlled fabrication of polyelectrolyte multilayer thin films using spin-assembly. Advanced Materials, 13(15):1167–1171, aug 2001.

[103] Paula T Hammond. Recent explorations in electrostatic multilayer thin film assembly. Current Opinion in Colloid & Interface Science, 4(6):430–442, dec 1999.

[104] S. Joly, R. Kane, L. Radzilowski, T. Wang, A. Wu, R. E. Cohen, E. L. Thomas, and M. F. Rubner. Multilayer nanoreactors for metallic and semiconducting particles. Langmuir, 16(3):1354–1359, feb 2000.

[105] Yutaka Ishimaru, Kazutoshi Arai, Masato Mizutani, Katsuhito Oshima, and Ikuho Iida. Physical and mechanical properties of wood after moisture conditioning. Journal of Wood Science,

47(3):185–191, jun 2001.

[106] R. Duplessix, M. Escoubes, B. Rodmacq, F. Volino, E. Roche, A. Eisenberg, and M. Pineri. Water absorption in acid nafion membranes. In ACS Symposium Series, pages 469–486. AMERICAN CHEMICAL SOCIETY, aug 1980.

[107] Tim J. Tambach, Peter G. Bolhuis, and Berend Smit. A molecular mechanism of hysteresis in clay swelling. Angewandte Chemie International Edition, 43(20):2650–2652, may 2004.

[108] Tim J. Tambach, Peter G. Bolhuis, Emiel J. M. Hensen, and Berend Smit. Hysteresis in clay swelling induced by hydrogen bonding: accurate prediction of swelling states. Langmuir, 22(3):1223–1234, jan 2006.

[109] J. M. O'Kane and D. C. Sherrington. Hysteresis-like behavior in the swelling/deswelling of polystyrene crosslinked resins using binary solvent mixtures. Macromolecules, 23(25):5286–5291, dec 1990.

[110] Ralf Kügler, Johannes Schmitt, and Wolfgang Knoll. The swelling behavior of polyelectrolyte multilayers in air of different relative humidity and in water. Macromolecular Chemistry and Physics, 203(2):413–419, jan 2002.

[111] Oleh M Tanchak, Kevin G Yager, Helmut Fritzsche, Thad Harroun, John Katsaras, and Christopher J Barrett. Water distribution in multilayers of weak polyelectrolytes. Langmuir, 22(11):5137–5143, 2006.

[112] Oleh M Tanchak, Kevin G Yager, Helmut Fritzsche, Thad Harroun, John Katsaras, and Christopher J Barrett. Ion distribution in multilayers of weak polyelectrolytes: A neutron reflectometry study. The Journal of chemical physics, 129(8):084901, 2008.

[113] Philip E. Ciddor. Refractive index of air: new equations for the visible and near infrared. Applied Optics, 35(9):1566, mar 1996.

[114] George M. Hale and Marvin R. Querry. Optical constants of water in the 200-nm to 200-um wavelength region. Applied Optics, 12(3):555, mar 1973.

[115] P. B. Johnson and R. W. Christy. Optical constants of the noble metals. Physical Review B, 6(12):4370–4379, dec 1972.

[116] Pedro J. Rivero, A. Urrutia, J. Goicoechea, and F.J. Arregui. Optical fiber humidity sensors based on localized surface plasmon resonance (lspr) and lossy-mode resonance (lmr) in overlays loaded with silver nanoparticles. Sensors and Actuators B: Chemical, 173(Supplement C):244 – 249, 2012.

[117] Brian J Melde, Brandy J Johnson, and Paul T Charles. Mesoporous silicate materials in sensing. Sensors, 8(8):5202–5228, 2008.

[118] Fernando Patolsky, Gengfeng Zheng, and Charles M Lieber. Fabrication of silicon nanowire devices for ultrasensitive, label-free, real-time detection of biological and chemical species. Nature protocols, 1(4):1711–1724, 2006.

[119] Michael C McAlpine, Habib Ahmad, Dunwei Wang, and James R Heath. Highly ordered nanowire arrays on plastic substrates for ultrasensitive flexible chemical sensors. Nature materials, 6(5):379–384, 2007.

[120] Frank Caruso, D Neil Furlong, Katsuhiko Ariga, Izumi Ichinose, and Toyoki Kunitake. Characterization of polyelectrolyte- protein multilayer films by atomic force microscopy, scanning electron microscopy, and fourier transform infrared reflection- absorption spectroscopy. Langmuir, 14(16):4559–4565, 1998.

[121] Dganit Danino and Yeshayahu Talmon. Direct-imaging and freeze-fracture cryo-transmission electron microscopy of molecular gels. Molecular Gels, pages 253–274, 2006.

[122] Alexander Wittemann, Markus Drechsler, Yeshayahu Talmon, and Matthias Ballauff. High elongation of polyelectrolyte chains in the osmotic limit of spherical polyelectrolyte brushes: a study by cryogenic transmission electron microscopy. Journal of the American Chemical Society, 127(27):9688–9689, 2005.

[123] Kell Mortensen and Yeshayahu Talmon. Cryo-tem and sans microstructural study of pluronic polymer solutions. Macromolecules, 28(26):8829–8834, 1995.

[124] Virender K Sharma, Ria A Yngard, and Yekaterina Lin. Silver nanoparticles: green synthesis and their antimicrobial activities. Advances in colloid and interface science, 145(1):83–96, 2009.